Applied Geochemistry 63 (2015) 116–132

Contents lists available at ScienceDirect

Applied Geochemistry

journal homepage: www.elsevier.com/locate/apgeochem

# Crystallization behavior of $NaNO_3$–$Na_2SO_4$ salt mixtures in sandstone and comparison to single salt behavior

Nadine Lindström, Nicole Heitmann, Kirsten Linnow, Michael Steiger*

*Department of Chemistry, University of Hamburg, Martin-Luther-King-Platz 6, 20146 Hamburg, Germany*

ARTICLE INFO

*Article history:*
Received 16 March 2015
Received in revised form
14 July 2015
Accepted 15 July 2015
Available online 3 August 2015

*Keywords:*
Salt weathering
Incongruently soluble double salts
Darapskite
Geochemical modeling
Raman microscopy
Salt crystallization
Crystallization pressure

ABSTRACT

We report on the crystallization behavior and the salt weathering potential in natural rock and porous stone of single salts ($NaNO_3$, $Na_2SO_4$) and salt mixtures in the ternary $NaNO_3$–$Na_2SO_4$–$H_2O$ system. Geochemical modeling of the phase diagram of the ternary $NaNO_3$–$Na_2SO_4$–$H_2O$ system was used to determine the equilibrium pathways during wetting (or deliquescence) of incongruently soluble minerals and evaporation of mixed electrolyte solutions. Experiments were carried out in order to study the phase changes during dissolution either induced by deliquescence or by the addition of liquid water. In situ Raman spectroscopy was used to study the phase transformations during wetting of pure $Na_2SO_4$ (thenardite) and of $Na_3NO_3SO_4 \cdot H_2O$ (darapskite). In both experiments crystallization of $Na_2SO_4 \cdot 10H_2O$ (mirabilite) from highly supersaturated solutions is demonstrated confirming the high salt weathering potential of thenardite and darapskite wetting. In order to study the damage potential of darapskite experimentally, wetting–drying experiments with porous sandstone with the two single salts ($Na_2SO_4$, $NaNO_3$) and two $NaNO_3$–$Na_2SO_4$ salt mixtures were carried out. Different destructive and non-destructive techniques were tested for damage monitoring. $NaNO_3$ was found to be the least damaging salt and $Na_2SO_4$ is the most damaging one. The classification of the two salt mixtures was less obvious.



## 1. Introduction

The weathering of natural rocks includes chemical weathering processes (mineral dissolution reactions) and processes of mechanical disintegration such as thermal stress, the swelling of clay minerals or crystal growth in confinement. Crystal growth is related to phase changes in pore solutions of natural rocks including the crystallization of the solvent (frost weathering) or of the solutes (salt weathering). The latter is considered as one of the most efficient agents of rock weathering in various environments (Goudie and Viles, 1997). Salt crystallization is also a major damage mechanism in porous building materials such as natural stone, brick or concrete.

Though chemical weathering and salt weathering are considered as different weathering mechanisms of rock breakdown, they generally operate together as the products of chemical dissolution reactions are more soluble than the parent minerals and are subsequently involved in dissolution–recrystallization cycles, then acting as the agents in salt weathering processes. For example, typical products of acid deposition to natural stone are mixtures of various sulfates and nitrates. Examples are calcium, sodium and magnesium sulfates. Due to their low solubility, massive accumulations of calcium sulfate minerals, especially gypsum ($CaSO_4 \cdot 2H_2O$) are commonly found in nature and also on natural building stones used as construction materials in polluted environments (Charola et al., 2007).

Other, more soluble sulfates, especially sodium sulfate and magnesium sulfate were found to be particularly efficient agents in salt weathering and the mode of action of these salts was subject of several investigations (e.g. Rodriguez-Navarro and Doehne, 1999; Flatt, 2002; Tsui et al., 2003; Espinosa Marzal and Scherer, 2008; Steiger et al., 2008a; Lopez-Arce et al., 2008; Balboni et al., 2011). There is now general agreement on the damage mechanism of these salts. Crystals growing in confined spaces can generate high stresses exceeding the tensile strengths of many materials if they grow under conditions of high supersaturation (Scherer, 2004; Steiger, 2005; Flatt et al., 2007).

Sodium sulfate is among those salts most widely used in laboratory studies of salt weathering including investigations in natural

* Corresponding author.
*E-mail address:* steiger@chemie.uni-hamburg.de (M. Steiger).

http://dx.doi.org/10.1016/j.apgeochem.2015.07.007
0883-2927/

rock weathering (Goudie and Viles, 1997) and in durability tests of building materials (e.g., RILEM Commission 25–PEM, 1980). Typically, in such tests a porous material is impregnated with a sodium sulfate solution and dried at enhanced temperature (e.g. 60–105 °C) such that one of the anhydrous polymorphs of $Na_2SO_4$, i.e. phase V (thenardite) and phase III, is formed. Subsequently, after cooling to room temperature, the specimen is impregnated again with a $Na_2SO_4$ solution leading to the hydration of $Na_2SO_4$. Repeating this procedure several times sodium sulfate proved to be extremely destructive and it was observed that most of the damage occurred during the impregnation phase. It is now generally accepted that the destructive effect is attributed to the growth of $Na_2SO_4 \cdot 10H_2O$ (mirabilite) crystals from the highly supersaturated solutions originating from the dissolution of anhydrous $Na_2SO_4$ (e.g. Flatt, 2002; Steiger and Asmussen, 2008; Flatt et al., 2014).

While the behavior of several single salts is well characterized, only few studies have been carried out on the crystallization behavior of salt mixtures in porous materials (e.g. Cardell et al., 2008; De Clercq, 2008; Lopez-Arce et al., 2008; Franzen and Mirwald, 2009; De Clercq et al., 2013). In the mixtures of sulfates and nitrates typically occurring in natural soil and rock and in building materials, several double salts may be formed such as $Na_2Mg(SO_4)_2 \cdot 4H_2O$ (bloedite), $K_3Na(SO_4)_2$ (glaserite) and $Na_3NO_3SO_4 \cdot H_2O$ (darapskite). Such salts show a complex crystallization behavior and Linnow et al. (2013) recently pointed out that these salts may have a great damage potential as they are incongruently soluble. Upon dissolution of an incongruently soluble compound the composition of the solution does not match that of the dissolved solid resulting in the formation of another solid. Therefore, upon dissolution, they behave similar to anhydrous sodium sulfate and lower hydrated magnesium sulfate phases and form a highly supersaturated solution. In the case of the single salts, this solution is supersaturated with respect to the respective higher hydrate; in the case of an incongruently soluble double salt, a solution supersaturated with one of the two single salt compounds is formed.

In this work, we study the behavior of $NaNO_3$–$Na_2SO_4$ mixed solutions including the formation of the incongruently soluble double salt darapskite. Darapskite is one of the more abundant minerals in the nitrate deposits found in dry environments such as the Atacama Desert, northern Chile (Ericksen, 1981), the Death Valley, southwestern United States (Ericksen et al., 1988), the Gobi Desert, northwestern China (Qin et al., 2012) and the Mc Murdo Dry Valleys, Antarctica (Keys and Williams, 1981). Darapskite is also a common mineral found in cave nitrates (e.g. Hill, 1981; Puşcaş et al., 2010). Finally, darapskite is often observed in efflorescences on building materials (e.g. Arnold and Zehnder, 1984; Holtkamp and Heinen, 1991; Nord, 1992; Matsukura et al., 2004).

In a previous paper, we have studied the crystallization of darapskite during evaporation of mixed salt solutions (Linnow et al., 2013). The present paper addresses the behavior of darapskite during wetting. In particular, we wanted to evaluate the damage potential of darapskite which is incongruently soluble. Upon wetting (or deliquescence), darapskite dissolves and forms a solution supersaturated with mirabilite. This implies that it may have a damage potential similar to sodium sulfate. In contrast, sodium nitrate, the other single salt in the ternary darapskite system, does not form different hydrated states. If it is subjected to a relative humidity (RH) above its deliquescence relative humidity (DRH), a solution is formed. If the humidity drops below the DRH, the salt crystallizes out again. No other phase changes except dissolution and recrystallization have to be considered.

There were three major objectives of this study: (1) Geochemical modeling of the phase diagram of the ternary $NaNO_3$–$Na_2SO_4$–$H_2O$ system was used to determine the equilibrium pathways during wetting (or deliquescence) and evaporation. (2) Experiments were carried out in order to study the phase changes during dissolution either induced by deliquescence or by the addition of liquid water. In situ Raman spectroscopy was used to study the phase transformations during wetting of pure $Na_2SO_4$ and of darapskite. One particular aspect of these experiments was to determine whether crystallization occurs under conditions of high supersaturation. (3) Wetting–drying experiments with porous sandstone contaminated with salt were carried out to determine the damage potential of darapskite. Sandstone samples, loaded with two different $NaNO_3$–$Na_2SO_4$ salt mixtures and with the respective single salts ($NaNO_3$, $Na_2SO_4$), were subjected to repeated cycles of wetting and drying. These experiments were carried out under more realistic conditions than in the conventional salt crystallization test (RILEM Commission 25–PEM, 1980), i.e. with much lower salt concentration that is not increased with every cycle. Different destructive and non-destructive techniques were tested for damage monitoring.

## 2. Materials and methods

### 2.1. Thermodynamic modeling

The calculation of solubilities in mixed electrolyte solutions requires equilibrium constants of the dissolution reaction for all solid species, i.e. their thermodynamic solubility products. For example, the solubility product of darapskite, $Na_3NO_3SO_4 \cdot H_2O$, is given by

$$\ln K_{dar} = 3\ln m_{Na} + \ln m_{NO_3} + \ln m_{SO_4} + 3\ln \gamma_{Na} + \ln \gamma_{NO_3} + \ln \gamma_{SO_4} + \ln a_w \quad (1)$$

where $m_{Na}$, $m_{NO_3}$, $m_{SO_4}$, $\gamma_{Na}$, $\gamma_{NO_3}$ and $\gamma_{SO_4}$ represent the molalities and activity coefficients of sodium, nitrate and sulfate, respectively, in the saturated solution and $a_w$ is the water activity of the saturated solution. The calculation of solubilities in mixed electrolyte solutions requires values of the solubility products $K_i$ of all solid phases $i$ in the temperature range of interest and the ability to calculate activity coefficients and water activities in mixed electrolyte solutions as a function of composition and temperature. An appropriate thermodynamic model to calculate the activity coefficients and the water activities in concentrated solutions as a function of composition and temperature is based on the Pitzer ion interaction formalism (Pitzer, 1991). For the present study we used the extended ion interaction model and the thermodynamic solubility products of thenardite, mirabilite, nitratine ($NaNO_3$) and darapskite reported previously (Steiger et al., 2008b). Values of the solubility products of the metastable phases of sodium sulfate, i.e., $Na_2SO_4$(III) and $Na_2SO_4 \cdot 7H_2O$, were taken from Steiger and Asmussen (2008).

### 2.2. Experiments

#### 2.2.1. Deliquescence of darapskite

Experiments were carried out to study the deliquescence behavior of darapskite by dynamic vapor sorption measurements. Pure darapskite was prepared as described previously (Linnow et al., 2013) and the vapor sorption measurements were carried out in a homemade setup with an analytical balance and a humidity generator (Linnow et al., 2014). Samples of approximately 50–100 mg were weighed into glass dishes. Care was taken to achieve an even distribution of single-grain layers on the bottom of the dishes. After placing the samples into the sorption balance, the

relative humidity was increased to the desired value in a single step. Subsequently, temperature and RH in the chamber and sample mass were continuously recorded until there was no further weight change which took up to 10 d at the highest humidity. The deliquescence humidity of darapskite calculated using our thermodynamic model is 80.7–80.9% at 20–25 °C (see Section 3.1), hence, vapor sorption experiments were carried out at 79%, 80%, 81%, 83% and 85% RH. Immediately after the water uptake was complete, Raman spectra of the samples were recorded to detect the phases present after equilibrium was achieved.

*2.2.2. Wetting–drying experiments with sandstone*

In order to investigate the damage potential of the two single salts and the salt mixtures during wetting, a test program was set-up. The conventional durability test of building materials and natural rocks with sodium sulfate (e.g. RILEM commission 25–PEM, 1980) did not seem to be appropriate for two reasons. First, the test is not realistic as the salt concentration increases with every cycle resulting in extremely high salt concentrations after few cycles. This might be useful to test the durability of materials which, however, is not the purpose of this study. Second, in the RILEM test the specimens are fully immersed in the salt solution to complete saturation and subsequently dried. Therefore, uncontrolled salt transport during impregnation and drying cannot be avoided which is possibly a problem if working with salt mixtures, e.g., by salt fractionation. Also, since we intend to keep the salt concentration realistically low, the cyclic impregnations have to be carried out with pure water. At low salt content however, the complete saturation of the pore space with water may lead to rather dilute solutions that may not be supersaturated any more. Therefore, a new test set-up was chosen in which the samples were impregnated with a salt solution only once. In the later cycles wetting was achieved by addition of a small amount of pure water.

The experiments were performed with samples (approx. 15 × 15 × 20 $mm^3$) of Sand sandstone (Middle Keuper, Late Triassic). The major constituents of the sandstone are quartz, rock fragments (chlorite clasts, hornblende, chert), plagioclase and alkali feldspars. Considerable amounts of clay minerals (mostly chlorite) are present as cementing material, argillaceous rock fragments, and as coatings filling the pores. From the dimensions of the stones and their weight densities were calculated yielding a value of $d = 2.10 \pm 0.06$ g $cm^{-3}$ which compares nicely to the literature value of 2.13 g $cm^{-3}$ (Grimm, 1990). The open porosity of Sand sandstone was determined by mercury intrusion porosimetry (MIP, see Section 2.3) and yielded $\phi = 0.197 \pm 0.001$ again in good agreement with the literature value ($\phi = 0.1999$) reported by Grimm (1990). The fresh sandstone has a pore-size distribution with modes at 0.05 μm, 4 μm, 12 μm and about 150 μm. The smallest pore sizes represent the intergranular pore space of clay mineral aggregates that are also responsible for the high values of hydric dilatation (Snethlage and Wendler, 1997) and the high cation exchange capacity of Sand sandstone (Schäfer and Steiger, 2002).

The surfaces of four sides of the stones were sealed with epoxy resin (each of the 15 × 20 $mm^2$ surfaces). Samples were then impregnated with salt solutions through one of the unsealed 15 × 15 $mm^2$ surfaces. In addition to single salt solutions of $Na_2SO_4$ (0.963 mol $kg^{-1}$ water) and $NaNO_3$ (1.45 mol $kg^{-1}$), two different $Na_2SO_4$–$NaNO_3$ mixed solutions were used. First, an equimolar mixed solution, solution I, (each salt: 1.15 mol $kg^{-1}$) was used, i.e. a solution with the same mixing ratio of the two salts as in the crystalline double salt. Following an equilibrium pathway, a solution of this composition would initially precipitate mirabilite which would redissolve on further evaporation forming darapskite (see Section 3.1). The second mixed solution, solution II, contained a substantial nitrate excess with a mole fraction of $NaNO_3$ of $x_{NO_3} = 0.9$ ($Na_2SO_4$: 0.287 mol $kg^{-1}$, $NaNO_3$: 2.46 mol $kg^{-1}$). Following the equilibrium pathway, this solution would first precipitate darapskite followed by nitratine (see Section 3.1). During impregnation the salt solutions were replaced five times to minimize effects of ion exchange processes. Sand sandstone contains large amounts of calcium and magnesium in exchangeable form (Schäfer and Steiger, 2002). Thus, impregnating this sandstone with a solution of a sodium salt causes the exchange of adsorbed calcium and magnesium with sodium resulting in a mixed pore solution also containing the respective calcium and magnesium salts. The total salt content in the specimens after the first impregnation–drying cycle was determined from the weight increase of the samples and yielded salt contents of (0.90 ± 0.04)% ($Na_2SO_4$), (0.75 ± 0.06)% ($NaNO_3$), (1.54 ± 0.04)% (solution I) and (1.64 ± 0.11)% (solution II). The uncertainties are standard deviations of the mean for 13 specimens of each series.

Samples were dried in a desiccator in a flow of dehumidified air (<10% RH) and subsequently weighed. During drying the underside of the samples was sealed using a paraffin sealing film (Parafilm). For wetting of the sample about 400 μL of doubly distilled water were added in portions using a microliter pipet. This amount of water is sufficient to completely fill the pore space of the specimens avoiding the formation of excess solution. During the first cycles, drying times were one week. Later, longer times were chosen to ensure complete drying. A total of 13 specimens were each treated with the same salt or salt mixture and initially subjected to the wetting–drying cycles not only to improve sampling statistics but also to provide a sufficient number of specimens for additional measurements with destructive techniques. The total number of cycles were 17 ($Na_2SO_4$ specimens) and 50 (all other specimens), respectively. In order to study the response of the clay mineral containing sandstone to wetting–-drying cycles, additional control experiments were carried out with salt-free samples. After 17 full cycles neither visible changes of the samples nor any detectable damage could be observed. After 14 cycles thin section analysis did not reveal any significant changes of the stone fabric. It is concluded that swelling of clay minerals does not interfere significantly with the results of the salt crystallization experiments.

The composition of the efflorescences on the stone surfaces was determined by Raman microscopy. Three specimens of each series were studied after the initial impregnation and drying and after four and seven cycles, respectively. These measurements were carried out in order to compare the crystallization of salts during evaporation with equilibrium pathways and with the crystallization sequences observed in our previous droplet evaporation experiments (Linnow et al., 2013) and the experiments with limestone specimens (De Clercq et al., 2013). Moreover, in the case of the salt mixtures, the composition of efflorescences may also indicate whether salt fractionation occurs as a result of precipitation of salts during capillary transport of the evaporating solution. For these measurements, the laser was focused at ten different spots on a half-diagonal of the exposed stone surface. Several other destructive and non-destructive techniques were used to evaluate the state of damage of the samples during the wetting–drying cycles. All samples were weighed after the drying phase of each cycle to determine continuously the material loss. Photographs of samples were taken regularly to monitor visual changes. Additional measurements that were performed include the determination of surface roughness and pore size distribution, the analysis of thin sections and the determination of the concentration and distribution of the ions in the specimens. Since some of these measurements are destructive, the number of specimens decreased during the program.

*2.2.3. In situ Raman spectroscopy during wetting*

Additional experiments using Raman spectroscopy were carried out to study the phase transitions during the wetting of the salt contaminated sandstone specimens in situ. In order to mimic the situation in the sandstone pores, samples were prepared as follows: A fresh sandstone sample was crushed and sieved to less than 500 μm. The powder was uniformly dispersed to the sticky surface of a carbon pad (normally used for SEM sample preparation) which was attached to a glass slide. Excess powder was removed and the residual monolayer of sandstone grains was then wetted with 1–3 droplets of the respective salt solution to obtain a uniform solution film. Droplets were evaporated in a flow of dry air and were then placed into the Raman microscope. First, the composition of the dry sample was determined. Subsequently, the sample was carefully wetted with 3–6 μL of doubly distilled water using a microliter pipet avoiding complete dissolution. Right after the addition of water Raman spectra were continuously recorded at the same spot of the sample surface.

## 2.3. Instrumentation

*2.3.1. Raman spectroscopy*

Raman spectra were recorded on a Senterra Raman dispersive microscope (Bruker Optics GmbH, Germany) with an automated Raman frequency calibration system (SurCal technology) using MPlan M 10× and LMPlanFL N 20× lens (Olympus Deutschland GmbH, Germany). The diode-laser excitation source was operated at 532 nm and 20 mW. Environmental conditions during the in situ measurements (Section 2.3) were monitored by using a capacitive humidity sensor HC2–CO5 and a Hygropalm AW2 indicator (Rotronic, Switzerland).

The Raman spectrum of a mixture of different solid phases can be expressed as the linear combination of the spectra of the pure compounds:

$$I(\lambda) = \sum_i b_i I_{r,i}(\lambda) \quad (2)$$

where $I(\lambda)$ is the intensity at wavelength $\lambda$ (the observed Raman spectrum) and $I_{r,i}(\lambda)$ are the reference spectra of the pure compounds $i$. The coefficients $b_i$ can be determined by ordinary least squares analysis using reference spectra of all compounds that might be formed in the system under investigation. Details on the measurements of the reference spectra are provided elsewhere (Linnow et al., 2013). The least squares analysis was carried out using a selected number of wavelengths at which the measured intensities in both the sample and the reference spectra were sufficiently high. The coefficients $b_i$ give the contributions of the reference spectra to the sample spectrum. No attempts were made to calibrate the method, i.e. the values of $b_i$ do not represent but are related to the mole fractions of compound $i$ in the sample.

*2.3.2. Mercury intrusion porosimetry*

Mercury intrusion porosimetry was used to detect changes in the total porosity and the pore size distribution of the sandstone. The measurements were performed using a PoreMaster 33 porosimeter (Quantachrome Instruments). Reference measurements were carried out on five samples of fresh Sand sandstone to obtain reference pore size distributions and pore volumes (see Fig. 1). In addition, six specimens treated with $Na_2SO_4$ and subjected to 17 complete wetting–drying cycles were used for MIP measurements. A set of three specimens was used directly after drying. Each of these specimens was cut into two pieces to conduct separate MIP measurements for both sides of the specimens, the upper side where water was added and evaporation occurred and the underside. Another set of three specimens was washed salt-free and then used for MIP measurements. These samples showed considerable sanding during the extraction of the salts and cutting of specimens was not possible. Samples from the remaining specimens treated with $NaNO_3$ and the mixed solutions were taken after 49 cycles (three samples for each treatment).

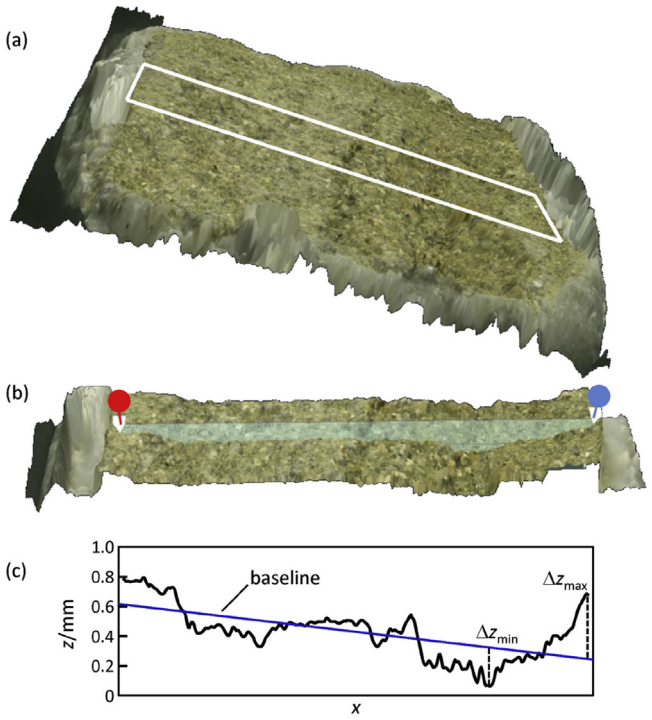


**Fig. 1.** Characterization of surface roughness from 3D images recorded using a digital microscope VHX-2000 with VH-20R zoom lens and controller VHX-S15 (Keyence). (a) upper surface of specimen treated with $Na_2SO_4$ after 17 cycles; (b) 3D image and position of one out of three line profiles; (c) diagram with line profile, baseline and distances $\Delta z_{max}$ and $\Delta z_{min}$.

*2.3.3. Microscopy*

Optical micrographs and topological images were recorded using a digital microscope VHX-2000 with VH-20R zoom lens and controller VHX-S15 for automatic profile measurement (Keyence). Surface roughness was determined from cross-sectional line profiles derived from three-dimensional images located at the center of the upper surface of the specimens and constructed with a resolution in $z$ direction of 10 μm. As an example, Fig. 1 shows the surface of a specimen treated with $Na_2SO_4$ solution after 17 wetting–drying cycles as described before. The marked area shown in Fig. 1a was used for the construction of a 3D image (Fig. 1b) from which line profiles were derived (three profiles for the treated specimens, five profiles for the fresh stones). The line profiles (example shown in Fig. 1c) were then used for the calculation of two-dimensional parameters for the characterization of surface roughness along the profiles. The root mean square roughness $Rq$ is given by

$$R_q = \sqrt{1/n \sum_{i=1}^{n} \Delta z^2} \quad (3)$$

where $\Delta z$ is the deviation of point $i$ on the profile line from the linear baseline which was determined by linear regression (blue line in Fig. 1c). A second parameter $R_z$ is the distance between the

highest peak ($\Delta z_{max}$) and the lowest valley ($\Delta z_{min}$) of the profile line (Fig. 1c), hence

$$R_z = \Delta z_{max} - \Delta z_{min} \quad (4)$$

Surface roughness measurements were carried out with two untreated stones and a specimen treated with $Na_2SO_4$ after 17 complete wetting–drying cycles. Surface roughness of stones treated with $NaNO_3$ and the two salt mixtures were carried out after 32 complete cycles. Due to the scatter observed in the roughness measurements the number of specimens investigated was increased in these cases. Three line profiles for each of six specimens were evaluated, i.e. a total of 18 line profiles for each treatment. In order to avoid mechanical damage during handling and undesirable changes on the surfaces of the specimens after the final drying cycle, they were not washed salt-free prior to the surface roughness measurements. However, the surfaces were carefully checked by optical microscopy with 200× magnification which confirmed that the surfaces are free from efflorescences. This is in agreement with the results of the ion analysis of the specimens (see Section 3.4). In addition to the roughness measurements, thin sections were also analyzed by optical microscopy.

#### 2.3.4. Measurement of salt content and distribution

Profiles of the concentrations of the major ions were determined in three stone samples of each series. In the case of the $Na_2SO_4$ specimens, measurements were carried out after 14 (one sample) and 17 cycles (two samples), respectively. In all other stones the salt distribution was determined after 14 (one sample) and 32 cycles (two samples). Specimens were dried at 60 °C (48 h), cut in slices of, typically, 2–5 mm, crushed and extracted with doubly distilled water. Cation concentrations in the extracts were measured using flame atomic spectrometry (Thermo Scientific iCE 3300). $Na^+$ and $K^+$ were determined in the emission-mode (F-AES) and $Mg^{2+}$ and $Ca^{2+}$ in absorption (F-AAS). Other cations than sodium were measured to determine whether ion exchange affected the composition of the salt mixture. However, $K^+$, $Mg^{2+}$ and $Ca^{2+}$ were not found in significant amounts. Concentrations of sulfate and nitrate in the aqueous extracts were determined by suppressed ion chromatography with conductivity detection (Dionex ICS 1000) using a 3.5 mmol $L^{-1}$ $Na_2CO_3$/1 mmol $L^{-1}$ $NaHCO_3$ eluent.

## 3. Results and discussion

### 3.1. Phase diagram of $NaNO_3$–$Na_2SO_4$–$H_2O$

The results of the solubility calculations in the system $NaNO_3$–$Na_2SO_4$–$H_2O$ using the model of Steiger et al. (2008b) are depicted in Fig. 2 and in Table 1 and compared to experimental data. Fig. 2a and b shows two isotherms at 20 °C and at 75 °C. The concentrations (molalities) of $NaNO_3$ and $Na_2SO_4$ in the solutions saturated with two solid phases (isobaric univariant equilibria) are shown in Fig. 3c and d. In general, there is excellent agreement between experimental and calculated solubilities. The diagrams show that darapskite, in the presence of a solution, can coexist with mirabilite at low temperature (curve 1 in Fig. 2c and d), with thenardite at high temperatures (curve 2) and with nitratine over the entire temperature range of its existence (curve 3). Darapskite is not stable in the presence of a solution at low temperature where no double salt is formed and mirabilite and nitratine coexist (curve 4). The intersection of curves 1, 3 and 4, is an isobaric invariant point ($NaNO_3$ + $Na_2SO_4{\cdot}10H_2O$ + $Na_3NO_3SO_4{\cdot}H_2O$ + solution). It is calculated at 13.8 °C. Likewise, darapskite is not stable at high temperature where thenardite and nitratine are the only stable phases (curve 5). The invariant point at the intersection of curves 2, 3 and 5 ($NaNO_3$ + $Na_2SO_4$(V) + $Na_3NO_3SO_4{\cdot}H_2O$ + solution) is calculated at 73.2 °C. Curve 6 represents the thenardite–mirabilite equilibrium in the ternary system which is shifted to lower temperatures in the presence of $NaNO_3$. This is the result of the decreasing water activity with increasing molality of $NaNO_3$. The invariant point at the intersection of curves 1, 2 and 6 represents a solution saturated with all three solids ($Na_2SO_4$(V) + $Na_2SO_4{\cdot}10H_2O$ + $Na_3NO_3SO_4{\cdot}H_2O$ + solution); it is calculated at 23.8 °C. Finally, the invariant point ($NaNO_3$ + $Na_2SO_4{\cdot}10H_2O$ + ice + solution) is the eutectic of the system, i.e., the lowest temperature at which a solution can exist. It is modeled at −17.5 °C.

In general, there is very good agreement of our calculated invariant equilibria with available literature data (Table 1). It is concluded that our model parameters allow for an accurate representation of the solubilities in the ternary system. It should be noted that the experimental data shown in Fig. 2 were used to determine the model parameters, thus, the calculated curves are not true model predictions. However, the predictive power of the model was demonstrated before (Steiger et al., 2008b) by accurate calculations of solubilities of darapskite and other solids in more complicated systems that were not used in the model parameterization.

A summary of the ternary solubility diagram illustrating the stability field of darapskite in the temperature–composition space is provided in Fig. 3a. As mentioned before, darapskite can only exist between 13.8 °C and 72.2 °C in the ternary system. In more complex systems, however, darapskite is stable also at lower temperatures. More important in the context of this research is the fact that darapskite is only stable in nitrate rich solutions with $0.76 < x_{NO_3} < 0.98$, i.e., darapskite is an incongruently soluble salt in the entire temperature range of its existence. This means that, whenever pure darapskite (i.e. $x_{NO_3} = 0.5$) is dissolved in a limited amount of water such that the resulting solution is still saturated with darapskite, this solution is supersaturated with respect to other solids, namely, thenardite and mirabilite at temperatures below 23.8 °C, or, only with respect to thenardite at higher temperatures. Therefore, as mentioned before, wetting of darapskite in a porous material such as natural rock or building stone may have a substantial damage potential due to crystal growth of mirabilite (or thenardite) from a highly supersaturated solution. The water required to dissolve an incongruently soluble salt in natural rocks or building stones may be supplied either by precipitation or condensation of water vapor on cold surfaces, or, by humidity cycling. Therefore, the deliquescence humidity (DRH) is an important property of an incongruently soluble salt. Fig. 3b depicts the incongruent DRH of darapskite as a function of temperature.

The experiments of this study were carried out under lab conditions without temperature control and temperature varied in a range from 20 to 25 °C. The solubility diagram of the system at a typical temperature of 23.5 C is shown in Fig. 4. The crystallization pathway of an equimolar mixed solution is depicted in Fig. 4a. Upon evaporation, solution I ($x_{NO_3} = 0.5$) reaches saturation with respect to mirabilite at point A. Following an equilibrium pathway, further evaporation causes the continuous crystallization of mirabilite, hence, the solution composition moves along the line A–$IP_1$ finally reaching the coexistence point $IP_1$ of mirabilite and darapskite which is an isothermal invariant point. $IP_1$ is also the drying point of solution I. At this point, mirabilite already precipitated should redissolve and darapskite should crystallize instead while the solution evaporates to dryness yielding pure darapskite as the final product.

It is well known that mirabilite nucleation is hindered and solutions that should precipitate mirabilite at equilibrium, often follow metastable crystallization pathways. Therefore, the

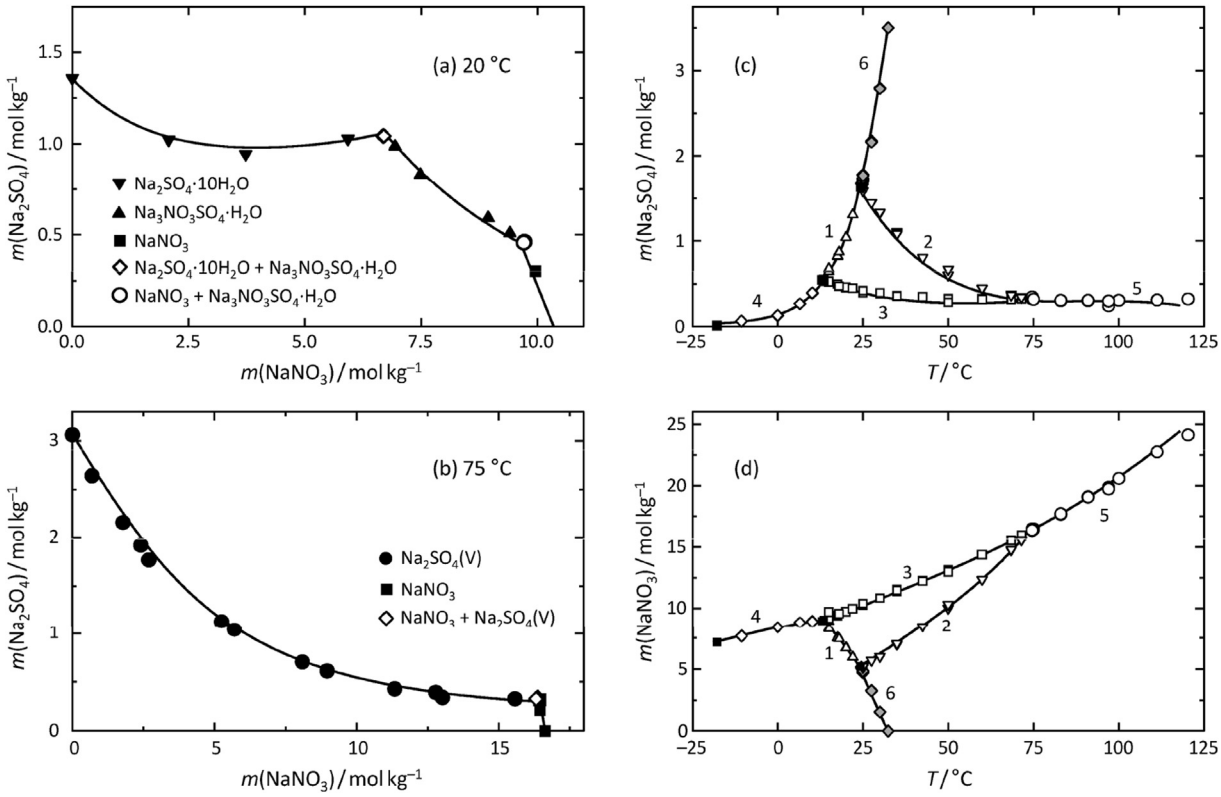


**Fig. 2.** Solubilities in the ternary system $NaNO_3$–$Na_2SO_4$–$H_2O$: Solubility isotherms at 20 °C (a) and 75 °C (b) and molalities of $Na_2SO_4$ (c) and $NaNO_3$ (d) at univariant equilibria. Lines are calculated solubilities and symbols represent experimental solubilities; meaning of symbols in (a) and (b) as indicated; symbols and numbered lines in (c) and (d) represent univariant equilibria and have the following meanings: (1) mirabilite + darapskite (triangles), (2) thenardite + darapaskite (inverted triangles), (3) nitratine + darapskite (squares), (4) mirabilite + nitratine (white diamonds), (5) thenardite + nitratine (circles), (6) thenardite + mirabilite (gray diamonds); black squares represent invariant points; experimental data taken from Foote (1925), Benrath (1928), Schröder (1929, 1930) and Chrétien (1929).

**Table 1**
Isobaric invariant points in the $NaNO_3$–$Na_2SO_4$–$H_2O$ system; experimental values (Chrétien, 1929; Foote, 1925) in brackets.

| Solid phases[a] | $T$/°C | $m(Na_2SO_4)$/mol·kg$^{-1}$ | $m(NaNO_3)$/mol·kg$^{-1}$ |
|---|---|---|---|
| (A) *ni* + *mi* + *dar* | 13.8 (13.0[b], 13.5[c]) | 0.56 (0.55[b], 0.54[c]) | 8.92 (8.95[b], 9.05[c]) |
| (B) *ni* + *th* + *dar* | 73.2 (–) | 0.30 (–) | 16.2 (–) |
| (C) *th* + *mi* + *dar* | 23.8 (24.3[b], 24.5[c]) | 1.62 (1.63[b], 1.67[c]) | 5.20 (5.18[b], 5.10[c]) |
| (D) *ni* + *mi* + *ice* | −17.5 (−17.8[c]) | 0.03 (0.01[c]) | 7.21 (7.14[c]) |

[a] *ni*: $NaNO_3$, *mi*: $Na_2SO_4 \cdot 10H_2O$, *th*: $Na_2SO_4$(V), *dar*: $Na_3NO_3SO_4 \cdot H_2O$.
[b] Literature sources are Chrétien (1929).
[c] Literature sources are Foote (1925).

metastable solubility branches of thenardite and darapskite are also shown in Fig. 4a. In addition to the phases mentioned so far, which may be stable or metastable depending on the solution composition, there are two additional phases of sodium sulfate, the heptahydrate ($Na_2SO_4 \cdot 7H_2O$) and a second anhydrous polymorph known as phase III, $Na_2SO_4$(III). Both phases are always metastable. Nonetheless, both solids were observed in laboratory experiments with sodium sulfate (Grossi et al., 1997; Rodriguez-Navarro et al., 2000; Linnow et al., 2006; Shahidzadeh-Bonn et al., 2008; Hamilton et al., 2008; Schiro et al., 2012; Saidov et al., 2012, 2015a). The solubilities of phase III and the heptahydrate are also shown in Fig. 4a.

The formation of the heptahydrate was typically observed in cooling experiments (Rijniers et al., 2005; Hamilton et al., 2008; Espinosa Marzal and Scherer, 2008). In this case, thenardite or phase III formation is not possible as their concentrations increase with decreasing temperature (Steiger and Asmussen, 2008). Thus, in the absence of mirabilite nucleation, the heptahydrate is the only metastable phase that can be precipitated upon cooling. The situation is different in the case of evaporation. If mirabilite crystallization does not occur, saturation with heptahydrate and the two anhydrous phases may be reached in an evaporating $Na_2SO_4$ solution. The solubility of the heptahydrate decreases rapidly with decreasing temperature whilst thenardite and phase III solubilities increase. Therefore, heptahydrate formation is more likely at low temperature while crystallization of the anhydrous phases should be favored at higher temperatures. In a pure $Na_2SO_4$ solution the heptahydrate–thenardite transition temperature is 24 °C (Steiger and Asmussen, 2008).

At temperatures close to the transition temperature both metastable phases have comparable solubilities (cf. lines 4 and 6 in Fig. 4a at zero $NaNO_3$ molality) and the question which one crystallizes first is a matter of the critical supersaturations and the experimental conditions affecting nucleation kinetics. This is confirmed by recent experimental findings. Saidov et al. (2015a) observed heptahydrate crystallization in a solution evaporated at

7.5 °C while thenardite was found at 25 °C. Schiro et al. (2012) observed heptahydrate formation during evaporation of a $Na_2SO_4$ solution from a porous substrate at 21–23 °C. Shahidzadeh-Bonn et al. (2008) carried out evaporation experiments with $Na_2SO_4$ solutions at 21 °C. They studied both droplet evaporation and evaporation from capillaries. Depending on the experimental conditions, they observed both initial formation of a hydrated phase (which was not further characterized) with subsequent dehydration and direct crystallization of both anhydrous salts (phase III and thenardite). In the course of our own droplet evaporation experiments we also observed the crystallization of the anhydrous salts from pure $Na_2SO_4$ solutions at 21–24 °C (Linnow et al., 2013).

Finally, it should be noted that under conditions of slow evaporation also mirabilite, the thermodynamically stable phase in the presence of a solution, may be precipitated first as observed by several authors (Rodriguez-Navarro and Doehne, 1999; Rodriguez-Navarro et al., 2000; Benavente et al., 2004). In conclusion, the question which of the four solids crystallizes first strongly depends on the experimental conditions.

The situation is different in ternary mixed $Na_2SO_4$–$NaNO_3$ solutions as solubilities of the various $Na_2SO_4$ phases are strongly affected by the $NaNO_3$ concentration, i.e. their solubilities decrease with increasing $NaNO_3$ molality. However, this effect is much more pronounced in case of the anhydrous salts than for the two hydrates (Fig. 4). In effect, with increasing $NaNO_3$ concentration the precipitation of the anhydrous salts is favored. For example, in an equimolar solution the solubility of thenardite is significantly lower than that of the heptahydrate and even phase III has a lower solubility. Finally, in the mixed system, darapskite solubility is also lower than that of the heptahydrate at high $NaNO_3$ molality, though its solubility is higher than that of thenardite in the equimolar solution (points B and C, respectively, in Fig. 4a). Nonetheless, in their droplet evaporation experiments with an equimolar mixed $NaNO_3$–$Na_2SO_4$ solution Linnow et al. (2013) found the direct crystallization of darapskite during evaporation corresponding to a metastable pathway following line A–C (Fig. 4a) where saturation with darapskite is reached. This pathway requires significant supersaturation with mirabilite (saturated at point A) and thenardite (saturated at B) but not in respect to phase III and the heptahydrate.

The equilibrium pathway for evaporation of solution II is also shown in Fig. 4a. It follows the dotted line for $x_{NO_3} = 0.9$ and reaches saturation with darapskite at point D. With ongoing crystallization of darapskite the solution composition follows the line D–$IP_2$ where saturation is reached with nitratine. $IP_2$ is the endpoint of the crystallization pathway of solution II, the remaining solution evaporates to dryness and both solids, darapskite and nitratine, are precipitated. In an evaporation experiment with a solution of similar composition, Linnow et al. (2013) noticed deviations from this equilibrium pathway and found the crystallization of the two solids in reversed order, i.e. implying significant supersaturation with darapskite and crystallization of nitratine. In

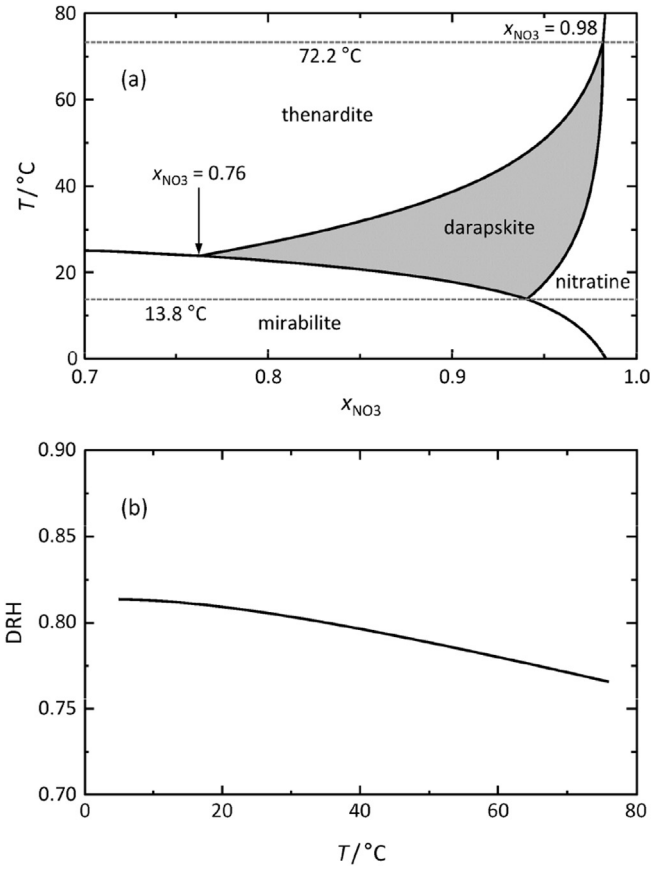


**Fig. 3.** (a) Calculated darapskite stability field as a function of composition and temperature; (b) calculated metastable (incongruent) deliquescence humidities of darapskite as a function of temperature.

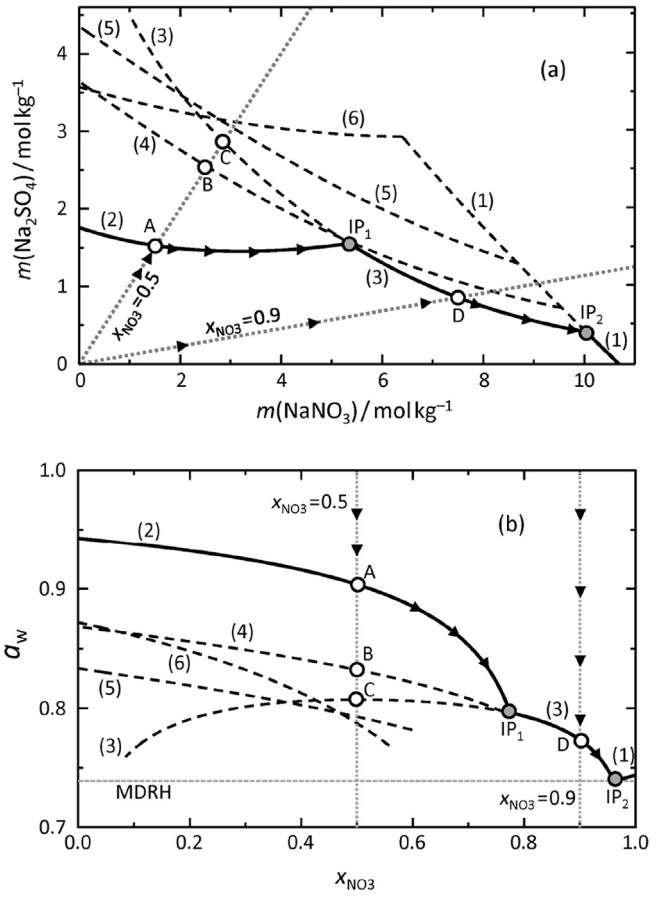


**Fig. 4.** Solubilities (a) and equilibrium water activities (b) in the system $NaNO_3$–$Na_2SO_4$–$H_2O$ at 23.5 °C. Solid and dashed curves denote stable and metastable equilibria, respectively, of nitratine (1), mirabilite (2), darapskite (3), thenardite (4), phase III (5) and heptahydrate (6); points $IP_1$ and $IP_2$ are the isothermal invariant points. Dotted lines represent the composition of the mixed solutions I ($x_{NO_3} = 0.5$) and II ($x_{NO_3} = 0.9$); arrows denote equilibrium crystallization pathways upon evaporation of these solutions; points A, B, and C represent saturation concentrations of mirabilite, thenardite and darapskite, respectively, in the equimolar mixed solution I; point D represents the saturation molality of darapskite in solution II.

conclusion, for both mixture compositions relevant to this study, the formation of phase III and of the heptahydrate phase is very unlikely during evaporation.

The equilibrium humidities of the saturated solutions are shown in Fig. 4b. The arrows denote the crystallization pathways of solutions I and II as described before (corresponding to Fig. 4a). The diagram also yields the equilibrium pathways for the deliquescence of the crystalline phases that are formed during evaporation of solutions I and II. The dry residue of solution II ($x_{NO_3} = 0.9$) is a mixture of mainly $NaNO_3$ and some $Na_3NO_3SO_4 \cdot H_2O$. The deliquescence of the salt mixture starts at 73.9% RH (23.5 °C) which is the saturation humidity of the solution with composition $IP_2$. In contrast to a single salt, deliquescence does not lead to complete dissolution of the salt mixture but rather to the dissolution of one of the components and partial dissolution of the other one. In the case of solution II, $NaNO_3$ is completely dissolved and $Na_3NO_3SO_4 \cdot H_2O$ only partially. The RH at which the deliquescence of a salt mixture starts is sometimes called the mutual deliquescence humidity, MDRH (Wexler and Seinfeld, 1991). Further increasing the RH above the MDRH, the second salt, of the mixture, $Na_3NO_3SO_4 \cdot H_2O$, is continuously dissolved until the endpoint of the deliquescence process is reached at point D. The deliquescence of the mixture is now complete. Thus, deliquescence of a salt mixture always occurs across a range of RH. In this particular case, with a large excess of one component of the mixture, this range is rather small. In other salt mixtures, especially in mixtures containing alkaline earth chlorides and nitrates, the RH range may be much broader (Steiger et al., 2015).

The equilibrium pathway of evaporation of solution I ($x_{NO_3} = 0.5$) ends with the formation of the pure double salt. In this particular case, though formed from a mixed salt solution, there is only one solid phase, hence, the deliquescence starts at the DRH of the double salt $Na_3NO_3SO_4 \cdot H_2O$ (point C). This point corresponds to the maximum of the saturation RH curve of darapskite. If this double salt were congruently soluble, this point would also be the endpoint of the deliquescence. However, since darapskite is incongruently soluble, the solution that is formed is supersaturated. It can be clearly seen from Fig. 4a and b that solution C at 23.5 °C is significantly supersaturated with thenardite and far supersaturated with mirabilite, however, it is not supersaturated with phase III and the heptahydrate. It can be also seen that there is an upper RH limit for the crystallization of mirabilite and thenardite which is given by the saturation humidities of these solids in an equimolar mixed solution (points A and B, respectively). If deliquescence of darapskite is carried out below these limiting values, deliquescence may be followed by the crystallization of either mirabilite or thenardite or both. This process is discussed in more detail in the following section.

### 3.2. Deliquescence of darapskite

The results of the deliquescence experiments with pure darapskite are depicted in Fig. 5. A typical curve of the water uptake with time after deliquescence of $Na_3NO_3SO_4 \cdot H_2O$ is shown in Fig. 5a (experiment at 83% RH). It is obvious that water uptake proceeds slowly. On the one hand, this is certainly due to the fact that the process was carried out at relative humidities only slightly above the DRH (cf. Linnow and Steiger, 2007). Moreover, it is expected that nucleation and growth of other phases may further hamper deliquescence and dissolution of darapskite. Nonetheless, a plateau was reached in all experiments. The total water content of the system at this moment in time, i.e. the amount of water picked up from the atmosphere plus the amount of water that was already present as water of crystallization in $Na_3NO_3SO_4 \cdot H_2O$, is plotted as a function of RH in Fig. 5b. It can be readily seen that deliquescence in fact occurs close to the calculated DRH of 80.7%.

At the end of the experiment Raman spectra of the samples were recorded. The results of these measurements are also indicated in Fig. 5b. At 79% and 80% RH only darapskite (*dar*) could be detected; a solution (*sol*) was detected for the first time at 81% but no other phases except darapskite. At 82%, darapskite could not be detected anymore and thenardite (*th*) appeared instead, but still in the presence of a solution. A saturated thenardite solution is also detected at 83%. Finally, at 85% the deliquescence is complete and no crystalline phase could be detected anymore.

In principle, these results confirm the expected complex deliquescence behavior of darapskite leading to supersaturation with respect to both thenardite and mirabilite. Although mirabilite is far more supersaturated, thenardite crystallization is observed. At first glance, this result is surprising as it is known that deliquescence of pure thenardite leads to the formation of mirabilite (Rodriguez-Navarro et al., 2000; Linnow et al., 2006, 2014; Desarnaud et al., 2013). The difference in the deliquescence of darapskite, however, lies in the fact that both phases mirabilite and thenardite are supersaturated. Again, the question which of the two solids crystallizes is controlled by the nucleation kinetics and depends on the

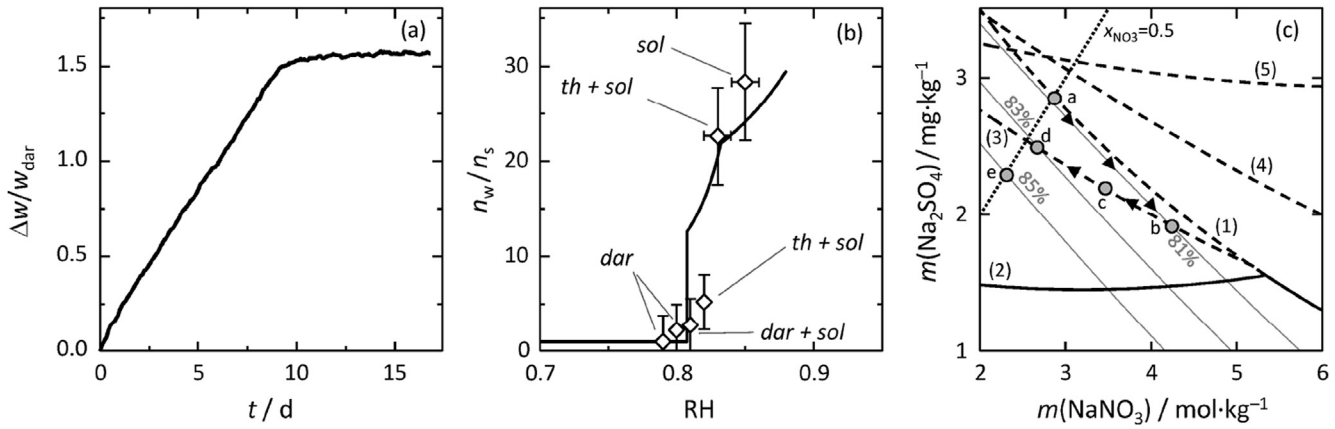


**Fig. 5.** Results of the deliquescence experiments with pure darapskite: (a) Typical water uptake vs. time curve (83% RH). (b) Equilibrium water content as a function of RH; symbols and error bars represent experimental data with estimated uncertainties in the determination of weight changes (vertical bars) and the precision of the humidity sensor used (horizontal bars, omitted at low RH for sake of clarity). (c) Detail of the solubility diagram at 23.5 °C (Fig. 4a) and proposed pathway of thenardite crystallization during deliquescence of darapskite (the meaning of points a–e is explained in the text).

experimental conditions. It is important to note that the actual supersaturation with respect to mirabilite is significantly lower in the darapskite saturated equimolar solution than in the thenardite saturated solution that formed during wetting of pure thenardite (see also discussion in Section in 3.5). Therefore, nucleation of mirabilite is less likely during wetting of darapskite than during wetting of thenardite.

A possible pathway of thenardite formation during deliquescence of darapskite is outlined in Fig. 5c which provides an enlarged view of the solubility diagram in Fig. 4a. For clarity, the solubility curves of the heptahydrate and of phase III are omitted as no supersaturation is reached with these solids. Also shown in Fig. 5c are lines of equal water activity (i.e., equilibrium humidity) at 81%, 83% and 85% RH. At the deliquescence point of darapskite (80.7%) a saturated equimolar mixed solution forms (solution a). At higher RH a more dilute solution is formed. During the deliquescence three different processes proceed at the same time: equilibration of the solution phase with the water vapor in the surrounding air, dissolution of darapskite and crystallization of thenardite. Assuming that dissolution and crystallization are slower than the vapor–liquid equilibration, the water activity will be nearly constant and in equilibrium with the RH of the air. Then, the composition of the solution will move along the corresponding line of constant water activity during thenardite crystallization until the supersaturation with thenardite is consumed. This pathway is indicated by the arrows in Fig. 5c for deliquescence at 81% RH. Reaching point b, the system is in an equilibrium state, darapskite is completely dissolved and part of the sodium sulfate crystallized out and is in equilibrium with a saturated solution at the equilibrium RH.

At other humidities the corresponding water activity lines intersect the solubility curve at different compositions, for instance at point c (82%) or at point d (83%). It should be noted that above 83.2% RH (23.5 °C) the water content is so high that an equimolar solution is not saturated any longer with thenardite. Thus, if the deliquescence of darapskite is carried out at such high RH no crystallization of thenardite occurs (for example, point e at 85% RH) which is in agreement with the experimental observation (Fig. 5b). It should be noted that the solution is still supersaturated with mirabilite under these conditions, however, no crystallization was observed in the present experiments. The calculated equilibrium water content of the system as a function of RH is also plotted in Fig. 5b. Considering the experimental uncertainties there is reasonable agreement with the theoretical water uptake.

### 3.3. Phase changes during wetting of anhydrous $Na_2SO_4$ and darapskite

Due to the fact that deliquescence did not, as originally assumed, lead to the crystallization of mirabilite, our further attempts to evaluate the damage potential of darapskite focused on wetting experiments with liquid water. In particular, it appeared necessary to investigate the phase transformations during wetting of darapskite by in situ Raman microscopy. Analogous experiments were also carried out with anhydrous $Na_2SO_4$ although the formation of mirabilite upon wetting of thenardite was demonstrated before by ESEM (Doehne, 1994; Rodriguez-Navarro et al., 2000), in situ XRD (Linnow et al., 2006) and X-ray analysis with synchrotron radiation (Espinosa-Marzal et al., 2011).

The results obtained for pure $Na_2SO_4$ are summarized in Fig. 6. The experiment was carried out at (23.2–23.6) °C and 33–36% RH. The diagram on the left depicts Raman spectra recorded right at the beginning and after the addition of water during a period of 27 min (increasing time from bottom to top). The vertical lines represent the peak positions of the totally symmetric stretching fundamental of the sulfate ion in the reference spectra of the various solids and of aqueous sulfate (Linnow et al., 2013). All spectra were evaluated as described in Section 2.3 to assess the composition of the samples. The results of these calculations are shown in the diagram on the right. The first spectrum (on the bottom) represents the dry crystalline salt mixture prior to the addition of water. The composition was found to be about 75% $Na_2SO_4$(V) and 25% $Na_2SO_4$(III). This is in good qualitative agreement with observations of Rodriguez-Navarro et al. (2000), Shahidzadeh-Bonn et al. (2008) and Linnow et al. (2013) who also found both anhydrous polymorphs (thenardite and phase III) in droplet evaporation experiments. It is unclear whether the anhydrous salts were formed in the present experiments by direct crystallization from solution, or, whether they were formed indirectly by dehydration of mirabilite. However, it is well known that mirabilite crystallization is inhibited and in our droplet experiments it was shown that the anhydrous phases crystallized directly from solution implying a substantial degree of supersaturation with mirabilite (Linnow et al., 2013) which was also observed by Rodriguez-Navarro et al. (2000) under conditions of rapid evaporation. Such a metastable pathway is also expected here due to the rapid drying at low relative humidity.

Upon addition of water, there is a significant change in the spectrum due to the dissolution of the two anhydrous phases and the formation of a hydrated phase. This is presumably $Na_2SO_4 \cdot 10H_2O$ as the formation of $Na_2SO_4 \cdot 7H_2O$ is very unlikely. The solubilities of $Na_2SO_4 \cdot 7H_2O$ and thenardite are very similar at 23.5 °C such that the dissolution of thenardite would not lead to sufficient supersaturation with the heptahydrate. It could have only formed upon dissolution of phase III. In the Raman spectra, it is not easy to distinguish heptahydrate and mirabilite as the symmetric stretching mode of the sulfate anion ($\nu_1$) is shifted by only about 2 $cm^{-1}$. Hamilton and Menzies (2010) report $\nu_1$ values of 989.3 $cm^{-1}$ (mirabilite) and 987.6 $cm^{-1}$ (heptahydrate). We have found values of 989.8 $cm^{-1}$ (Linnow et al., 2013) and 988.3 $cm^{-1}$ (Linnow et al., 2014). This makes it difficult to distinguish the two solids if they are both present. This is unlikely, however, as it is well-known that the metastable heptahydrate rapidly transforms into mirabilite once nucleation of the latter occurred (Espinosa Marzal and Scherer, 2008; Hamilton and Menzies, 2010; Hamilton et al., 2008; Schiro et al., 2012; Saidov et al., 2015b). In addition to the $\nu_1$ symmetric stretch also the $\nu_2$ bending and, especially, the $\nu_3$ asymmetric stretch modes are helpful to distinguish the spectrum of heptahydrate from those of mirabilite and aqueous sulfate which have very similar spectra. In the pure heptahydrate spectrum, the $\nu_3$ stretch shows a distinct doublet at 1103.9 $cm^{-1}$ and 1134.6 $cm^{-1}$. These values are in good agreement with values of 1106.6 $cm^{-1}$ and 1134.9 $cm^{-1}$ reported by Hamilton and Menzies (2010). The absence of this doublet and the Raman shift of the $\nu_1$ mode both indicate, in agreement with thermodynamic considerations, that the heptahydrate did not form in our wetting experiment.

Once it is accepted that mirabilite is the hydrated phase formed, the Raman spectra recorded during the first six minutes after the addition of water confirm the presence of $Na_2SO_4 \cdot 10H_2O$, $Na_2SO_4$(V) and an aqueous solution. This solution is presumably highly supersaturated with respect to $Na_2SO_4 \cdot 10H_2O$. The maximum supersaturation during the growth of the $Na_2SO_4 \cdot 10H_2O$ crystals corresponds to the solubility of thenardite. After about six minutes a solution can no longer be detected by Raman spectroscopy although the presence of small films cannot be ruled out. In absence of a solution, the mirabilite initially formed is not stable at such low relative humidities and dehydration should occur. In fact, the Raman spectra provide evidence for rapid dehydration of mirabilite and formation of thenardite and a small fraction of phase III.

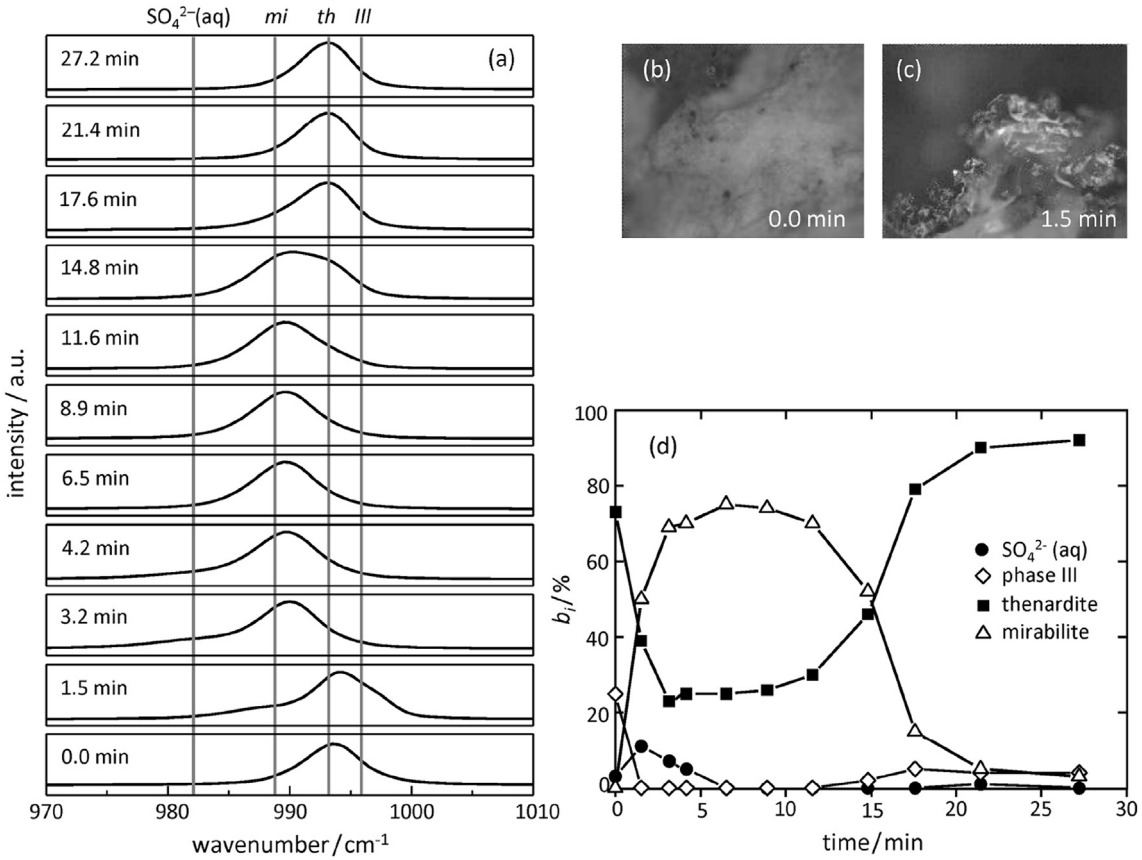


**Fig. 6.** Raman spectra (a), micrographs (b, c) and approximate composition (d) of sample during wetting of anhydrous $Na_2SO_4$. Vertical lines represent peak positions of the totally symmetric stretching fundamental of the sulfate tetrahedra in aqueous sulfate (982.1 $cm^{-1}$), mirabilite (988.8 $cm^{-1}$), thenardite (993.2 $cm^{-1}$) and phase III (995.9 $cm^{-1}$).

This process starts about 12 min after the addition of water and is finished after about 22 min. Finally, the end product of the cycle is anhydrous $Na_2SO_4$. These measurements provide clear evidence for the damage mechanism discussed in detail earlier by Flatt (2002), Tsui et al. (2003), Steiger and Asmussen (2008) among others. Raman spectra confirm the growth of mirabilite under conditions of very high supersaturation. Since thenardite is still present during the growth of mirabilite, the crystallization pressure generated by the growing mirabilite crystals can be calculated assuming that the solution is saturated with thenardite. This calculation yields a crystallization pressure of 10.0 MPa at 23.5 °C (Steiger and Asmussen, 2008).

The experiments with the equimolar mixed $NaNO_3$–$Na_2SO_4$ solution are more complicated. The results of the in situ Raman measurements during a single wetting–drying cycle are shown in Fig. 7. The evaluation of the Raman spectrum of the initial dry salt mixture reveals the presence of $Na_3NO_3SO_4 \cdot H_2O$ (~50%), $NaNO_3$ (~35%) and about 15% anhydrous $Na_2SO_4$ (mainly thenardite) which is in good agreement with the composition of the efflorescences on the sandstone surfaces after the initial drying (see Section 3.4). However, the presence of three different solid phases is not in agreement with the phase rule and can only be explained by a metastable crystallization pathway and fractionation during drying of the samples. This is again due to the inhibited mirabilite crystallization yielding sufficiently high concentrations during evaporation to reach saturation with thenardite and $Na_3NO_3SO_4 \cdot H_2O$ (points B and C in Fig. 4a) and most likely with $Na_2SO_4$(III) as well.

The Raman spectra recorded after the addition of water to the salt mixture confirm the partial dissolution of the solids and the formation of a mixed solution. All $NaNO_3$ and a large fraction of $Na_3NO_3SO_4 \cdot H_2O$ are rapidly dissolved whilst it appears that anhydrous $Na_2SO_4$ largely remains in crystalline form. This is in agreement with the solubility diagram. Nitratine dissolves first followed by darapskite and the composition of the solution moves along the saturation curve of darapskite. If the amount of water is limited, thenardite is not dissolved in a darapskite saturated solution at mixing ratios close to equimolar (see Fig. 4a). This solution is far supersaturated with mirabilite. In fact, the precipitation of mirabilite starts simultaneously with the dissolution of darapskite and nitratine. In the further course of the reaction several processes proceed simultaneously. Mirabilite dehydrates and darapskite recrystallizes from the remaining mixed solution. It also appears that consumption of crystalline anhydrous $Na_2SO_4$ by dissolution and formation of darapskite on the one hand, is nearly compensated by its formation through dehydration of mirabilite on the other hand. In conclusion, the damage mechanism for the mixed $NaNO_3$–$Na_2SO_4$ solution is similar to that of pure $Na_2SO_4$. The dissolution of a metastable crystalline solid (metastable if in contact with water) yields a supersaturated solution with mirabilite.

It is difficult to assess the degree of supersaturation in this mixed solution. It follows from the Raman spectra (Fig. 7) that mirabilite growth occurred in the presence of both anhydrous $Na_2SO_4$ phases. This implies that the minimum concentration of the solution must have been saturation with $Na_2SO_4$(III). The exact mixing ratio of sulfate and nitrate in this solution is not known. Considering however, that about half of the darapskite and all nitratine dissolved during the wetting of the sample the mixing ratio may be roughly estimated to fall between a value of $x_{NO_3} = 0.5$ (dissolution of pure darapskite) and $x_{NO_3} = 0.66$ (dissolution of about equal amounts of darapskite and nitratine). For these two

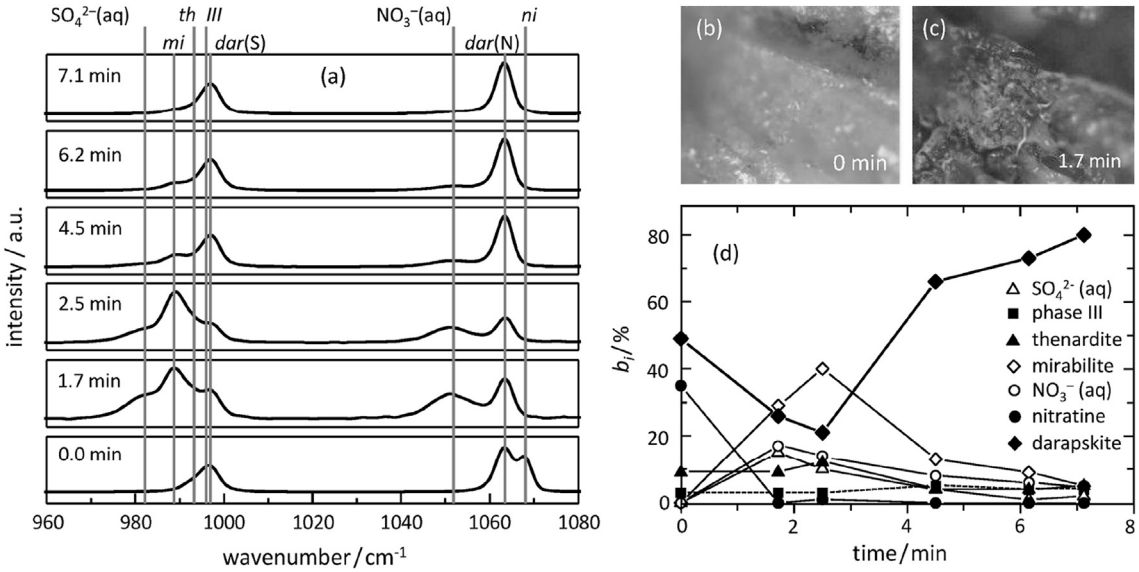


**Fig. 7.** Raman spectra (a), micrographs (b, c) and composition (d) of sample during wetting of salt mixture I. Vertical lines represent peak positions of the totally symmetric stretching fundamentals of the sulfate and nitrate ions; $SO_4^{2-}$(aq) (982.1 $cm^{-1}$), mirabilite: *mi* (988.8 $cm^{-1}$), thenardite: *th* (993.2 $cm^{-1}$), phase III: *III* (995.9 $cm^{-1}$), $NO_3^-$(aq) (1051.8 $cm^{-1}$), nitratine: *ni* (1068.1.9 $cm^{-1}$), darapskite: *dar* (sulfate: 997.0 $cm^{-1}$, nitrate: 1063.4 $cm^{-1}$).

compositions we have calculated the molalities in the solutions saturated with $Na_2SO_4$(III). Calculation of the supersaturation with mirabilite and of the resulting crystallization pressure for these concentrations yields values of 6.3 MPa for $x_{NO_3} = 0.5$ and 3.4 MPa for $x_{NO_3} = 0.66$ at 23.5 °C. Though the calculated crystallization pressure is lower, the damage mechanism is the same as for pure $Na_2SO_4$. The reason for the smaller crystallization pressure is the decreasing solubility of the anhydrous phases with increasing nitrate concentration (Fig. 4). In contrast, mirabilite solubility is nearly independent of the sodium nitrate concentration. In effect, the supersaturation with mirabilite of a solution saturated with an anhydrous phase decreases with increasing nitrate content yielding a smaller crystallization pressure of mirabilite in the $Na_2SO_4$(III) saturated mixed solution compared to pure $Na_2SO_4$.

### 3.4. Wetting–drying experiments

#### 3.4.1. Efflorescences

After the initial impregnation and drying procedure, the upper surfaces of all specimens were partially covered with efflorescences. Especially on the specimens impregnated with $Na_2SO_4$ solution, a dense and thick efflorescence layer covered the stone surface. With increasing number of cycles the amount of efflorescences rapidly decreased and only little efflorescences were visible after the third cycle. After more than 7 cycles the surfaces of most specimens appeared nearly free of efflorescences. The surfaces of the specimens treated with $NaNO_3$ solution, were free of efflorescences already after the third cycle. The decrease in the amount of salt on the top surface of all samples with increasing number of wet–dry cycles is the result of salt transport into the interior and to the bottom of the specimens as discussed below. In addition, a loss of efflorescences from the specimens was observed due to blow-off in the strong dry air flow during drying. Blow-off was especially noticeable in the case of the samples loaded with sodium sulfate which were coated with particularly thick and fluffy efflorescences. The loss of these efflorescences reduces the salt concentration in the samples and, thus, the damage potential.

The main constituents in the efflorescences on the sandstone samples treated with the single salt solutions as detected by Raman microscopy were $NaNO_3$ (nitratine) and $Na_2SO_4$(V) (thenardite). It was surprising that anhydrous phase III was not detected in the efflorescences on the specimen treated with sodium sulfate. In the droplet evaporation experiments on glass slides (Linnow et al., 2013) $Na_2SO_4$(III) was found to be the main product. Phase III was also detected after evaporation of a solution droplet on the carbon pads covered with stone powder, however, thenardite was far more abundant (see Fig. 6). In the efflorescences on the stone surfaces phase III was observed after the seventh cycle in two out of three samples. These results imply that both anhydrous phases can be formed during evaporation on the sandstones surfaces as also observed in capillary and droplet evaporation experiments (Rodriguez-Navarro and Doehne, 1999; Linnow et al., 2013); the higher supersaturation necessary for the nucleation of phase III requires high evaporation rates that might not be always reached during the drying of the stone specimens. Though unlikely, a precipitation sequence involving mirabilite formation and subsequent dehydration cannot be ruled out, however.

The main constituents in efflorescences formed during initial drying of the specimens impregnated with mixed solution I were $Na_3NO_3SO_4 \cdot H_2O$, $Na_2SO_4$(V) and $NaNO_3$ again indicating a crystallization pathway far from equilibrium resulting in the formation of more solid phases than predicted by the phase rule. Also in this case, the results are different from those obtained for droplet evaporation from glass slides where the double salt darapskite was detected as the only solid. However, the same phases were obtained after drying a droplet of solution I on the covered carbon pad (Fig. 7). The results also agree qualitatively with those of De Clercq et al. (2013) who also found complex mixtures of several compounds in efflorescences formed on limestones during evaporation of an equimolar mixed $NaNO_3$–$Na_2SO_4$ solution. According to them the drying conditions (mainly RH) and the properties of the porous support strongly affect the drying behavior and the composition of efflorescences. The analysis of the efflorescences after the third and the seventh cycle revealed similar results. The only difference is the presence of phase III in significant amounts in the later cycles just as in the case of the samples treated with pure $Na_2SO_4$.

The only compound that could be detected in the efflorescences formed during the first evaporation of solution II ($x_{NO_3} = 0.9$) was

$NaNO_3$. For stoichiometric reasons a sulfate phase must be also present which could not be detected by Raman spectroscopy however. This might be simply due to the very low concentrations of darapskite or thenardite (or both) and the poor sampling statistics. It is also possible that sulfate containing phases crystallized later during the evaporation and, therefore, formed subflorescences that are not detectable by Raman spectroscopy. In the efflorescences after the third and the seventh cycle, darapskite could be detected as well but still no $Na_2SO_4$ phase.

*3.4.2. Salt content and distribution*

With increasing number of cycles salt efflorescences were observed on the underside of the samples confirming the transport of salts from the top surface (where the water was added) to the bottom. This transport of the salts was also confirmed by the profiles of the ion contents. In all samples that were investigated (3 specimens of each series) a strong accumulation of the salts on the bottom surface was observed. This implies that, despite of the covering of the surface with paraffin film during the drying of the samples, there must have been some evaporation through the bottom surface which is responsible for this enrichment and the formation of efflorescences also on the bottom side. Considering that the maximum stress generated by growing crystals during both wetting and drying is reached in the pores with the highest salt concentration (the maximum degree of pore filling), it is concluded that there was a shift of the position of maximum stress from the upper surface (during the first cycles) to the lower surface (with increasing number of cycles).

Comparing the analysis of the soluble salt measurements with the results of the weight of the samples after the first impregnation and drying cycle, confirmed that blow-off of the efflorescences in the air flow of the drying chamber caused a loss of about 71% of the initial salt content in the specimens treated with $Na_2SO_4$. In the other samples losses of 32%, 25% and 21% were observed in the specimens treated with $NaNO_3$ and with solutions I and II, respectively.

*3.4.3. Weight loss*

Weight loss curves of the samples treated with the four salt solutions are shown in Fig. 8. Sample mass is plotted as $w/w_0$ where $w$ is the weight after each drying cycle and $w_0$ is the weight of the untreated dry stone. Each point represents the average relative weight of the samples treated with the same salt. The error bars are the standard deviations of the mean. Initially, there were 13 samples of each series, however, the number decreased during the program due to the destructive measurements that were carried out (MIP, ion analysis, thin sections). The total number of specimens in each series is also indicated in Fig. 8. The value $w/w_0$ of the stones after the initial impregnation with salt (i.e. cycle number 0) is given by the squares. It is obvious that there is a substantial increase in the weight of the samples after the first wetting–drying cycle. This weight increase is due to residual moisture in the samples (incomplete drying) and is also the main reason for the cyclic behavior of the sample weights. Whenever the specimens were dried longer than usual, lower weights were determined and a weight increase was observed in the subsequent cycles due to the enrichment of residual moisture. At the end of the experiments the drying times were increased to 4 weeks resulting in smoother weight loss curves.

The samples treated with the $NaNO_3$ solution only show a small weight change during the 50 cycles. In addition to the residual water content due to incomplete drying, the weight loss curves are also affected by a partial loss of salt due to the blow-off of efflorescences (32% of the initial salt content in the case of $NaNO_3$). Considering these influences, the overall decrease in the weight loss curve of the specimens treated with $NaNO_3$ is hardly significant. This is confirmed by the determination of the dry masses of specimens that were used after 32 and 50 cycles, respectively, for the determination of the salt content and for MIP measurements. The dry weights of these samples after complete removal of residual moisture did not show any significant weight decrease. This appears to be consistent with the damage mechanism expected for the samples treated with $NaNO_3$. In contrast to sodium sulfate or the two salt mixtures, sodium nitrate can only cause damage during the drying phase when nitratine crystallizes out provided that both supersaturation and the pore filling are sufficient. During the wetting phase, nitratine simply dissolves but no other crystalline phases are formed. The content of $NaNO_3$ in the specimens after the initial treatment is moderate to low and about 32% of the initial salt content is lost during the experiments. Nothing can be said about the supersaturation that is reached during evaporation and growth of $NaNO_3$ pore solutions. However, together with the low salt concentration the supersaturation was obviously too low to cause severe damage and material loss during the experiments.

In contrast to sodium nitrate, damage in the experiments with sodium sulfate is largely attributed to the dissolution of anhydrous $Na_2SO_4$ during the wetting phase and subsequent crystallization of the decahydrate under conditions of high supersaturation. This damage process causes a significant loss of material which is clearly visible in the weight loss curves even though they are affected by residual moisture and blow-off of salt efflorescences. The average $w/w_0$ value of the samples that were completely dried after the last cycle was found to be 0.996. Further considering the contribution of the blow-off of efflorescences to the overall weight loss, a net material loss after only 17 cycles is evident.

The weight loss curves for the stones treated with the two mixed solutions show a similar trend of slightly decreasing weight. Though this trend is significantly less pronounced than in the case of $Na_2SO_4$, it appears to be significant compared to $NaNO_3$. In the case of solution II which should behave similar to pure $NaNO_3$, i.e. damage is only expected during evaporation drying, this might be the result of the higher total salt concentration compared to the samples treated with pure $NaNO_3$. In the case of the equimolar mixture (solution I), the greater weight loss appears to be a reasonable result as crystal growth of mirabilite during wetting is expected. However, in comparison to the much higher weight loss of the stones treated with $Na_2SO_4$, the result obtained for the specimens treated with solution I is surprising. Assuming that the same damage mechanism holds and considering that the total salt content is even higher than in the $Na_2SO_4$ specimens, more damage, i.e. a more significant weight loss, could have been expected in the case of the samples treated with solution I. The higher weight loss of the $Na_2SO_4$ samples is an indication that darapskite may be less damaging than $Na_2SO_4$ despite of the same damage mechanism. There is another obvious feature of the weight loss curves of the specimens treated with solution I. The sample weights show significantly larger scatter than for all other specimens. This could be an indication of a stronger influence of stone inhomogeneities on the damage process in the case of darapskite crystallization as discussed in more detail in Section 3.5. Finally, it should be noted that most of the weight loss of the specimens treated with the equimolar mixed solution occurred during the first about 18 cycles. This is, most likely, the result of salt transport from the top surface of the specimens (which is the wetted surface) to the bottom where efflorescences formed. It is possible that a significant fraction of the salt mixture is not reached anymore by the water added from the top such that the actual damage process is not active anymore in the later cycles.

It is also surprising that the weight loss curves of the specimens treated with solution II show a similar behavior than those treated

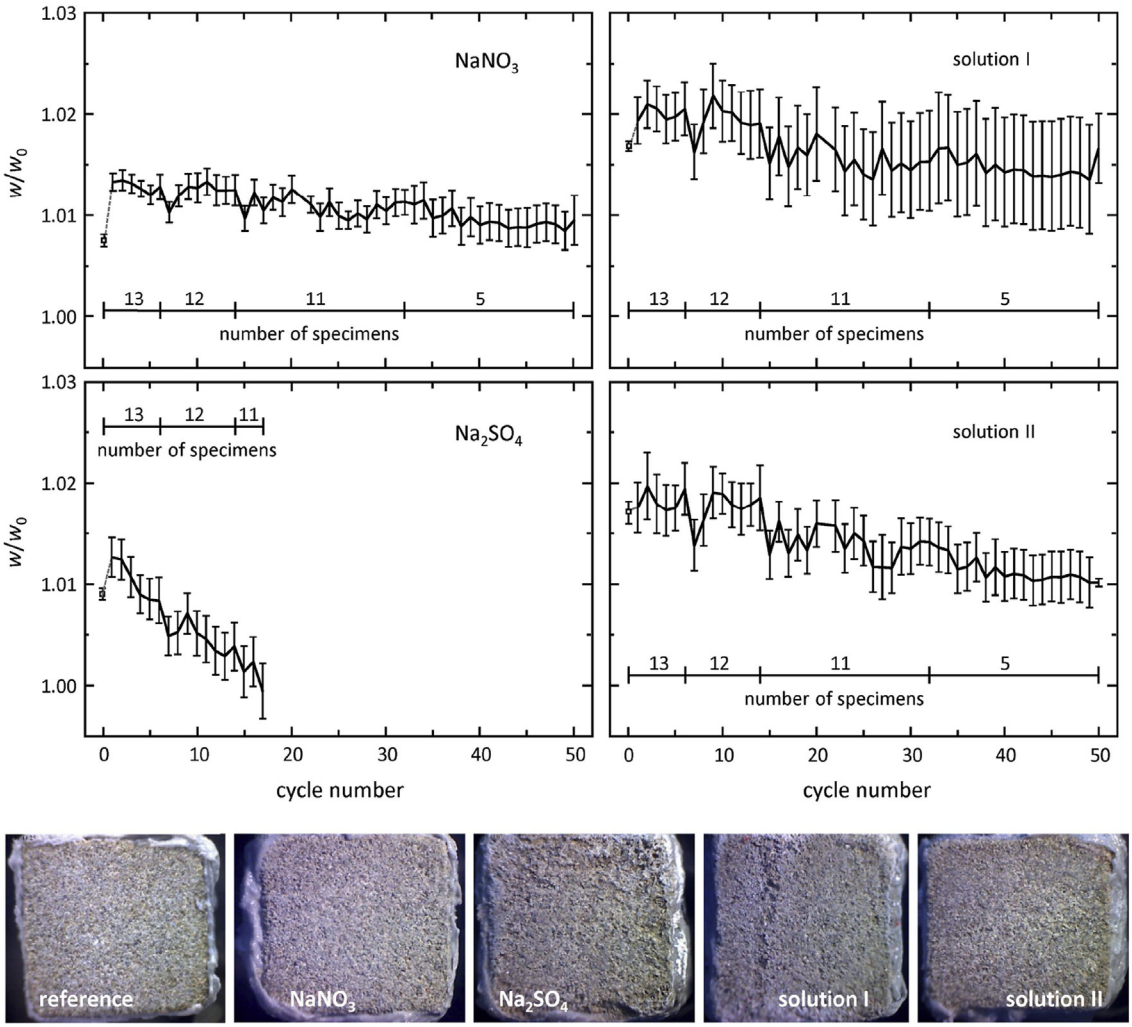


**Fig. 8.** Average relative weight loss curves of stone samples treated with $NaNO_3$, $Na_2SO_4$ and mixed solutions I and II. Error bars are standard deviations of identically treated samples (number of specimens as indicated). Symbols represent values of $w/w_0$ after the initial impregnation and complete drying; the value at cycle number 0 represents the weight increase after impregnation with the respective salt solution. The photographs show the upper surfaces of an untreated reference and of specimens treated with $NaNO_3$, $Na_2SO_4$ and solutions I and II after 7 wetting–drying cycles.

with the equimolar solution I. Due to the large excess of $NaNO_3$ in the former specimens, there is only a rather small amount of anhydrous $Na_2SO_4$ present that might lead to mirabilite supersaturation and growth. Therefore, it was expected that stones treated with mixed solution II should show similar behavior than those impregnated with pure $NaNO_3$. The main difference between the samples is the much higher $NaNO_3$ content in the specimens treated with the mixed solution II. In contrast, the $Na_2SO_4$ content is so low that mirabilite formation due to dissolution of $Na_2SO_4$ or darapskite is a less likely damage mechanism. It is, therefore, assumed that the more pronounced weight loss in these samples is due to the higher pore filling and crystallization of nitratine during drying.

In order to compare the weight loss results with visual observations, Fig. 8 also shows photographs of the upper surfaces of an untreated reference stone and of specimens treated with $NaNO_3$, $Na_2SO_4$ and solutions I and II after 7 wetting–drying cycles. The classification derived from the weight loss curves is confirmed by the visual inspection of the stone surfaces. The specimens treated with $Na_2SO_4$ clearly showed the most pronounced surface changes, the least damage is visible on the specimens treated with $NaNO_3$ followed by mixed solution II, more damage is observed on the specimens treated with the equimolar mixed solution I. However, different stones treated with solution I clearly showed different damage intensities in agreement with the larger scatter in the weight loss curves.

### 3.4.4. Surface roughness, porosity and pore size distribution

As an attempt to quantify visual changes, surface roughness measurements were carried out. The results of these measurements are summarized in Fig. 9. Average values of $R_q$ and $R_z$ for the fresh reference samples and the specimens treated with $Na_2SO_4$, $NaNO_3$ and the two mixed solutions are shown in Fig. 9a and b. Compared to the original surface of Sand sandstone there is an increase in roughness on the top surface of all stones subjected to wetting–drying cycles confirming the visual observations. It should be noted that the measurements with the $Na_2SO_4$ specimen which showed the most pronounced increase in roughness were carried out after 17 cycles whilst all other measurement were carried out after 32 cycles. In other words, about half of the total number of cycles resulted in significantly more surface damage in case of the $Na_2SO_4$ specimens.

The error bars shown in Fig. 9a and b represent the standard deviations of the mean values of $R_q$ and $R_z$. In some cases there is

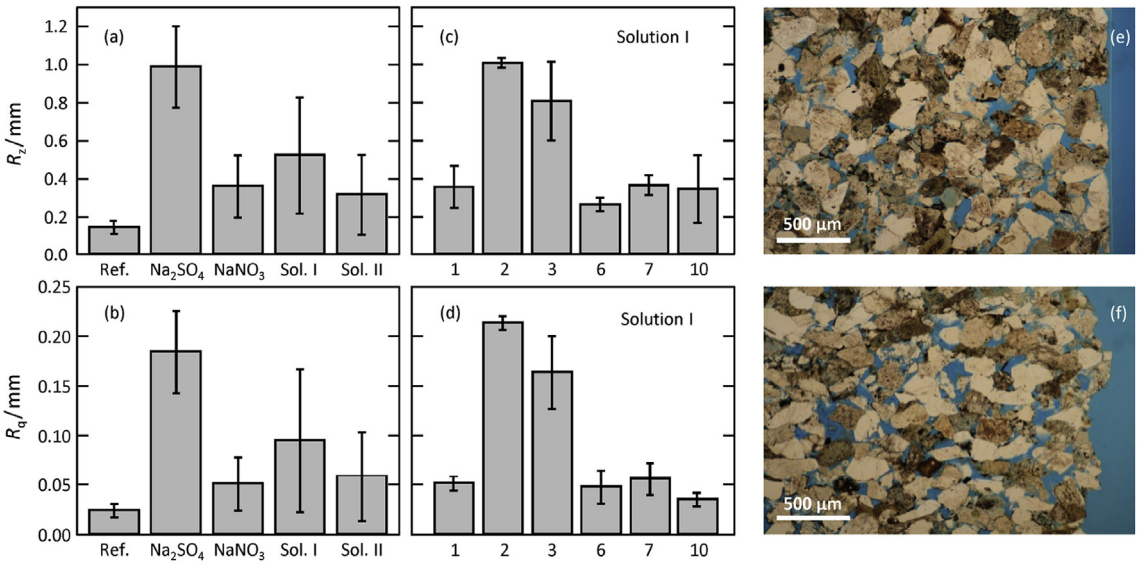


**Fig. 9.** Surface roughness of untreated Sand sandstone and specimens subjected to wet–dry cycles. Left diagrams: roughness parameters $R_z$ (a) and $R_q$ (b) of two untreated reference samples (Ref.) and of specimens treated with $Na_2SO_4$ (1 specimen, after 17 cycles), $NaNO_3$ and mixed solutions I and II (6 specimens each, after 32 cycles); right diagrams: $R_z$ (c) and $R_q$ (d) values of six specimens of the series treated with an equimolar mixed salt solution (solution I); micrographs: thin sections of untreated Sand sandstone (e) and a specimen treated with $Na_2SO_4$ after 17 cycles (f).

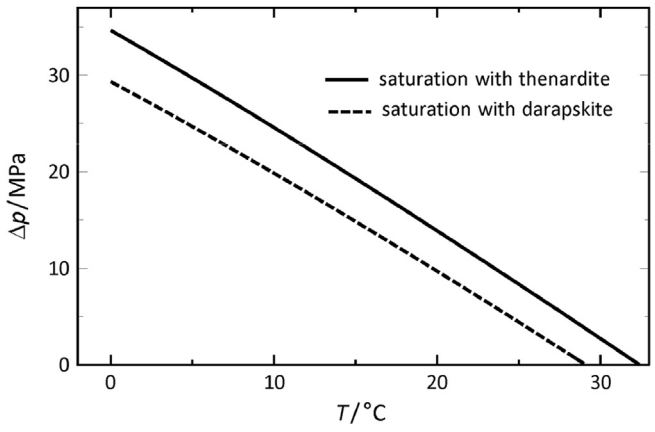


**Fig. 10.** Maximum crystallization pressure as a function of temperature generated by mirabilite crystals growing from solutions saturated with thenardite (solid line, taken from Steiger and Asmussen, 2008) and darapskite (dashed line).

large scatter reflecting significant variability of the values of $R_q$ and $R_z$ as determined from different line profiles. Particularly large scatter was observed for the 6 specimens treated with the equimolar mixed solution I. Fig. 9c and d depict a more detailed view on these measurements. Each of the bars represents the average roughness parameters of the respective specimen. The error bars represent the standard deviations of the mean values obtained from the evaluation of three line profiles for each specimen. It is obvious that there is significant scatter, in particular, the differences between different specimens treated in the same way and subjected to the same number of wetting–drying cycles is striking and confirms the scatter of the weight loss curves and the visual observations of samples treated with solution I. For example, specimens 2 and 3 show an increased surface roughness that is comparable with the specimen treated with $Na_2SO_4$ shown in Fig. 9a and b. The large values determined for specimens 2 and 3 are the main cause of the large standard deviations of $R_z$ and $R_q$ shown in Fig. 9a and b. Such large scatter reflects the inhomogeneities of both the fabric of the sandstone samples and the salt distribution within the pores. Some samples can have higher pore fillings close to the surface than others. If this is combined with surface zones of lower strength large differences in surface roughness may evolve. Therefore, roughness parameters shown in Fig. 9a and b have to be interpreted with some care. Nonetheless, the average results are in good qualitative agreement with the ranking derived from the visual inspection of the specimens.

An increase in surface roughness is the result of damage on the stone surface caused by the loss of individual mineral grains or larger fragments due to salt crystallization. However, changes in the stone fabric in depth, e.g. the formation of cracks, may also be a cause of increased surface roughness. This is illustrated in Fig. 9e and f where thin section photomicrographs of an untreated reference specimen (Fig. 9e) and that of a $Na_2SO_4$ specimen after 17 cycles (Fig. 9f) are compared. In comparison to the original flat surface of the untreated stone (Fig. 9e), the stone treated with $Na_2SO_4$ has an irregular rough surface. In this case however, the surface roughness is not the result of the loss of single grains or grain aggregates but rather reflects a change in the fabric close to the surface with loss of cohesion at grain contacts and newly formed porosity that caused the irreversible movement of grains resulting in buckling of the originally flat surface.

In order to detect changes in the stone fabric underneath the surface, MIP is an appropriate technique as salt enrichment and formation of cracks affect porosity and pore size distribution (PSD). A useful discussion on possible changes in the PSD of building stones affected by salt damage is provided by Angeli et al. (2008). The MIP measurements of the specimens treated with $Na_2SO_4$ revealed an increase of the open porosity detectable with MIP from 19.7 ± 0.1 in four fresh samples (see Section 2.1) to an average porosity of 20.8 ± 1 in 3 specimens after 17 cycles of wetting–drying and subsequent extraction of the salt. This is in agreement with the idea that salt crystallization leads to the formation of cracks and the creation of new porosity. However, upon closer inspection and considering the reproducibility of the measurements, the differences are not significant. In fact, average porosities determined in other specimens without removal of the salts were even larger (21.1 ± 0.9). In other words, the scatter in the

measured porosities is too large due to material inhomogeneity and uneven salt distribution. Moreover, sample sizes required for the MIP measurement are too large, thus, formation of few cracks, e.g. formed close to the surfaces of the stones, is not sufficient to alter significantly the average porosity and average PSD in the whole sample volume. For the same reasons, also the minor changes in the PSD of weathered and fresh samples are not significant and no definite conclusions can be drawn regarding the pore size dependence of the salt distribution and crack sizes formed.

### 3.5. Damage potential of darapskite

The present experiments confirm that the same damage mechanism as in the case of wetting of $Na_2SO_4$ also applies to darapskite. Just as thenardite, darapskite, an incongruently soluble double salt, is not stable in the presence of liquid water. Both salts dissolve resulting in a highly supersaturated solution with mirabilite. However, the experiments have also shown that wetting of thenardite is more damaging than wetting of darapskite. For example, in the wetting–drying experiments the specimens loaded with 0.9% (by weight) of pure $Na_2SO_4$ showed significantly more damage after only 17 cycles than the specimens initially loaded with 0.97% $Na_2SO_4$ plus 0.58% $NaNO_3$ after 50 cycles.

The generation of high stresses that are sufficient to cause damage requires two conditions to be met, supersaturation and confinement. Whether the crystals do grow against pore walls and can generate stress, depends on the degree of pore filling. The more salt is accumulated in the pore and the larger the contact area of the growing crystals with the pore wall is (under conditions of supersaturation), the higher the stress. The pore filling is similar in the experiments with $Na_2SO_4$ and with the $Na_2SO_4$–$NaNO_3$ mixture and it is not expected that such small differences can be responsible for the observed differences in the evolution of damage. The supersaturation during the growth of mirabilite in our experiments may be estimated from the respective solubility diagrams as discussed before and can be used to calculate the resulting crystallization pressures. Such calculations yielded crystallization pressures of mirabilite at 23.5 °C of 10 MPa for dissolution of pure $Na_2SO_4$ and about 3.4–6.3 MPa for dissolution of darapskite. This difference in the crystallization pressure is the likely reason for the higher damage potential of pure sodium sulfate compared to darapskite during wetting. The differences in the crystallization pressures are caused by the different influence of the $NaNO_3$ concentration on the solubilities of mirabilite and darapskite as discussed in Section 3.2.

The lower crystallization pressure in combination with inhomogeneities of salt distributions might also explain the large differences in weight loss curves and surface roughness that were observed for different specimens treated with solution I. The example shown on the photograph in Fig. 8 confirms that also material inhomogeneities largely affect the weathering behavior of sandstone. It is possible that at low pore fillings the lower crystallization pressures generated by dissolution of darapskite can only damage zones of lower strength in the sandstone such as the weak layer in the specimen shown in Fig. 8.

Considering the results of all measurements and the visual inspection, it is also questionable whether the specimens treated with solution I are more damaged than those impregnated with solution II. However, it is important to note that darapskite and, most likely, other incongruently soluble double salts have a higher damage potential than single salts that do not form higher hydrated states such as NaCl (above 0 °C), $NaNO_3$ and $KNO_3$ as they can cause damage also during wetting. It is also important to note that the damage potential of darapskite (and of $Na_2SO_4$) depends strongly on temperature and increases with decreasing temperature. The reason for this behavior is the strong influence of temperature on the solubility of mirabilite. While the solubility of mirabilite decreases with temperature, the solubility of thenardite increases. Therefore, the supersaturation with mirabilite upon wetting of thenardite increases with decreasing temperature leading to a significant increase in the maximum crystallization pressure (Steiger and Asmussen, 2008) which is illustrated in Fig. 10. Though there is a slight decrease in the solubility of darapskite with decreasing temperature, the supersaturation is again largely controlled by the much stronger solubility decrease of mirabilite. Therefore, the crystallization of mirabilite growing from a solution saturated with darapskite also increases at low temperature as depicted in Fig. 10. In conclusion, the damage potential of darapskite is much higher at low temperature and similar damage as with sodium sulfate may be expected.

## 4. Conclusions

Using a Pitzer type electrolyte solution model the solubilities of the ternary system $NaNO_3$–$Na_2SO_4$–$H_2O$ are successfully modeled yielding excellent agreement with experimental data. Based on the complete phase diagram also including metastable equilibria the various possible crystallization pathways during both evaporation from mixed solutions and wetting of the double salt darapskite, $Na_3NO_3SO_4 \cdot H_2O$, can be analyzed and compared to experimental findings. The phase diagram confirms that metastable crystallization pathways and the incongruent solubility of darapskite lead to the formation of metastable phases and result in a rather complex phase change behavior of this simple ternary system. A high theoretical damage potential is predicted from the phase diagram for the wetting of darapskite.

In the case of wetting with liquid water, this is confirmed by the in situ Raman microscopy experiments. In these experiments, it is shown that dissolution of darapskite goes hand in hand with mirabilite crystallization in the presence of crystalline anhydrous $Na_2SO_4$, i.e. under conditions of high supersaturation. Therefore, the damage mechanism during wetting of darapskite is very similar to the well known damage mechanism of pure sodium sulfate, i.e. wetting of thenardite. However, the degree of supersaturation is lower in the case of darapskite wetting resulting in a lower theoretical crystallization pressure. In the case of wetting by deliquescence, no mirabilite formation is observed.

In order to study the damage potential of darapskite experimentally, wetting–drying experiments with porous sandstone were carried out. One of the objectives of the study was to use more realistic experimental conditions in these aging tests by using lower salt concentrations not increasing with every cycle as in the conventional $Na_2SO_4$ crystallization test. Under less drastic conditions of an aging test not necessarily leading to complete breakdown of samples after a limited number of cycles, the detection of the early stages of the damage turned out to be a critical issue. Problems related to the selection of appropriate assessment methods in aging tests were discussed recently by several authors (e.g. Angeli et al., 2007; Lubelli et al., 2014). The main problem with the visual observation is its subjectivity that does not allow for a quantitative description of the state of alteration. This was also a problem in the present study. However, none of the experimental techniques used for a quantitative determination of the state of damage, i.e. monitoring of the weight of samples, measurement of surface roughness and mercury intrusion porosimetry, lead to an unambiguous classification of the two single salts and the two salt mixtures regarding their damage potential. The problem in weight loss measurements is always the ambiguity that weight changes can be related to material loss but also to changes in the salt and moisture content. Similarly, also the surface roughness and MIP

measurements were hardly significant considering the scatter of the data.

Despite of these problems, there is no doubt that pure $NaNO_3$ is the least damaging salt tested. This can be easily understood as $NaNO_3$ is the only salt in this study that cannot cause damage during wetting. Under such conditions it is simply dissolved without crystallization of other compounds. Therefore, $NaNO_3$ can only cause damage during the drying phase in wetting–drying experiments. The experiments also unambiguously demonstrated that $Na_2SO_4$ is the most damaging salt. Without doubt, this is due to the crystallization of mirabilite at high supersaturation during wetting. It is also clearly demonstrated with the present experiments that this well-known damage mechanism is also very efficient under more realistic experimental conditions, especially with significantly lower salt loads. The classification of the two salt mixtures was much more difficult. The equimolar mixed solution leading to the formation of darapskite upon drying was expected to be more damaging due to the high damage potential during wetting of the double salt. However, this could not be unambiguously demonstrated in the present experiments. Though significant damage was observed in some specimens there was large scatter. In contrast, the mixed solution with a large $NaNO_3$ excess also resulted in more damage than pure $NaNO_3$. Although there is some potential for mirabilite crystallization from this mixture, the main salt is nitratine and damage should preferably occur during the drying phase when $NaNO_3$ crystallizes. Therefore, the higher damage potential compared to pure $NaNO_3$ is most likely the result of the much higher salt load in the specimens treated with this mixed solution. In conclusion, the theoretically high damage potential of darapskite that was clearly demonstrated in the in situ wetting experiments is not yet unambiguously confirmed within porous materials. Thus, further work is required, for example, with higher salt loads and at lower temperatures. Such work is in progress and will be the subject of a future report.

## Acknowledgment

This research was funded by the Deutsche Forschungsgemeinschaft (DFG, STE 915/6-1). The authors would like to thank Jamie Yeoh (Keyence Deutschland GmbH) for help with the surface roughness measurements and Hans-Hermann Neumann for help with the thin section photomicrographs.

## References

Angeli, M., Bigas, J.-P., Benavente, D., Menéndez, B., Hébert, R., David, C., 2007. Salt crystallization in pores: quantification and estimation of damage. Environ. Geol. 52, 205–213.

Angeli, M., Benavente, D., Bigas, J.-P., Menéndez, B., Hébert, R., David, C., 2008. Modification of the porous network by salt crystallization in experimentally weathered sedimentary stones. Mater. Struct. 41, 1091–1108.

Arnold, A., Zehnder, K., 1984. Evaporite und Verwitterung am Bauwerk. Eclogae Geol. Helv. 77, 287–300.

Balboni, E., Espinosa-Marzal, R.M., Doehne, E., Scherer, G.W., 2011. Can drying and re-wetting of magnesium sulfate salts lead to damage of stone? Environ. Earth Sci. 63, 1463–1473.

Benavente, D., Garcia del Cura, M.A., Garcia-Guinea, J., Sanchez-Moral, S., Ordonez, S., 2004. Role of pore structure in salt crystallization in unsaturated porous stone. J. Cryst. Growth 260, 532–544.

Benrath, A., 1928. Über das reziproke Salzpaar $MgSO_4$–$Na_2(NO_3)_2$–$H_2O$. I. Z. Anorg. Chem. 170, 257–287.

Cardell, C., Benavente, D., Rodríguez Gordillo, J., 2008. Weathering of limestone building material by mixed sulfate solutions. Characterization of stone microstructure, reaction products and decay forms. Mater. Charact. 59, 1371–1385.

Charola, A.E., Pühringer, J., Steiger, M., 2007. Gypsum: a review of its role in the deterioration of buildings materials. Environ. Geol. 52, 339–352.

Chrétien, A., 1929. Étude du système quaternaire. Eau, nitrate de sodium, chlorure de sodium, sulfate de sodium. Ann. Chim. 12, 9–155.

De Clercq, H., 2008. Behaviour of limestone contaminated with binary mixtures of sodium sulphate and treated with a water repellent. Int. J. Restor. Build. Monum. 14, 357–364.

De Clercq, H., Jovanovic, M., Linnow, K., Steiger, M., 2013. Performance of limestone laden with $Na_2SO_4$–$NaNO_3$ and $Na_2SO_4$-$K_2SO_4$ mixtures. Environ. Earth Sci. 69, 1751–1761.

Desarnaud, J., Bertrand, F., Shahidzadeh-Bonn, N., 2013. Impact of the kinetics of salt crystallization on stone damage during rewetting/drying and humidity cycling. J. Appl. Mech. 80, 020911.

Doehne, E., 1994. In situ dynamics of sodium sulfate hydration and dehydration in stone pores: observations at high magnification using the environmental SEM. In: Fassina, V., Ott, H., Zezza, F. (Eds.), The Conservation of Monuments in the Mediterranean Basin. Proceedings of the 3rd International Symposium. Graffo, Venice, pp. 143–150.

Ericksen, G.E., 1981. Geology and Origin of the Chilean Nitrate Deposits. In: Geological Survey Professional Paper 1188. United States Government Printing Office, Washington DC.

Ericksen, G.E., Hosterman, J.W., Amant, P.S., 1988. Chemistry, mineralogy and origin of the clay-hill nitrate deposits. Amargosa river valley, Death Valley region, California, U.S.A. Chem. Geol. 67, 85–102.

Espinosa Marzal, R.M., Scherer, G.W., 2008. Crystallization of sodium sulfate salts in limestone. Environ. Geol. 56, 605–621.

Espinosa-Marzal, R., Hamilton, A., McNall, M., Whitaker, K., Scherer, G.W., 2011. The chemomechanics of crystallization during rewetting of limestone impregnated with sodium sulfate. J. Mater. Res. 26, 1472–1481.

Flatt, R.J., 2002. Salt damage in porous materials: how high supersaturations are generated. J. Cryst. Growth 242, 435–454.

Flatt, R.J., Steiger, M., Scherer, G.W., 2007. A commented translation of the paper by C.W. Correns and W. Steinborn on crystallization pressure. Environ. Geol. 52, 187–203.

Flatt, R.J., Caruso, F., Aguilar Sanchez, A.M., Scherer, G.W., 2014. Chemo-mechanics of salt damage in stone. Nat. Commun. 5 (5), 4823. http://dx.doi.org/10.1038/ncomms5823.

Foote, H.W., 1925. The system sodium nitrate-sodium-sulphate-water, and the minerals darapskite and nitroglauberite. Am. J. Sci. 9, 441–447.

Franzen, C., Mirwald, P.W., 2009. Moisture sorption behavior of salt mixtures in porous stone. Chem. Erde 69, 91–98.

Goudie, A., Viles, H., 1997. Salt Weathering Hazards. John Wiley & Sons, Chichester.

Grimm, W.D., 1990. Bildatlas wichtiger Denkmalgesteine der Bundesrepublik Deutschland. Karl M. Lipp Verlag, München.

Grossi, C.M., Esbert, R.M., Suárez del Rio, L.M., Montato, M., Laurenzi-Tabasso, M., 1997. Acoustic emission monitoring to study sodium sulphate crystallization in monumental porous carbonate stones. Stud. Conserv. 42, 115–125.

Hamilton, A., Menzies, R.I., 2010. Raman spectra of mirabilite, $Na_2SO_4 \cdot 10H_2O$ and the rediscovered metastable heptahydrate, $Na_2SO_4 \cdot 7H_2O$. J. Raman Spectrosc. 41, 1014–1020.

Hamilton, A., Hall, C., Pel, L., 2008. Sodium sulfate heptahydrate: direct observation of crystallization in a porous material. J. Phys. D Appl. Phys. 41, 212002.

Hill, C.A., 1981. Mineralogy of cave nitrates. Nat. Speleol. Soc. Bull. 43, 127–132.

Holtkamp, M.H.P.C., Heijnen, W.M.M., 1991. The mineral darapskite in the efflorescences on two Dutch churches. Stud. Conserv. 36, 175–178.

Keys, J.R., Williams, K., 1981. Origin of crystalline, cold desert salts in the McMurdo region, Antarctica. Geochim. Cosmochim. Acta 45, 2299–2309.

Linnow, K., Zeunert, A., Steiger, M., 2006. Investigation of sodium sulfate phase transitions in a porous material using humidity and temperature controlled X-ray diffraction. Anal. Chem. 78, 4683–4689.

Linnow, K., Steiger, M., 2007. Determination of equilibrium humidities using temperature and humidity controlled X-ray diffraction (RH-XRD). Anal. Chim. Acta 583, 197–201.

Linnow, K., Steiger, M., Lemster, C., De Clercq, H., Jovanović, M., 2013. In-situ Raman observation of the crystallization in $NaNO_3$–$Na_2SO_4$–$H_2O$ solution droplets. Environ. Earth Sci. 69, 1609–1620.

Linnow, K., Niermann, M., Bonatz, D., Posern, K., Steiger, M., 2014. Experimental studies of the mechanism and kinetics of hydration reactions. Energy Proced. 48, 394–404.

Lopez-Arce, P., Doehne, E., Martin, W., Pinchin, S., 2008. Magnesium sulfate salts and historic building materials: experimental simulation of limestone flaking by relative humidity cycling and crystallization of salts. Mater. Construcc. 58, 125–142.

Lubelli, B., van Hees, R.J.P., Nijland, T.G., 2014. Salt crystallization damage: how realistic are existing ageing tests?. In: 3rd International Conference on of Salt Weathering of Buildings and Stone Sculptures H. De Clercq). The Royal Institute for Cultural Heritage, Brussels, pp. 259–273.

Matsukura, Y., Oguchi, C.T., Kuchitsu, N., 2004. Salt damage to brick kiln walls in Japan: spatial and seasonal variation of efflorescence and moisture content. Bull. Eng. Geol. Environ. 63, 167–176.

Nord, A., 1992. Efflorescence salts on weathered building stone in Sweden. Geol. Fören. Stockh. Förh. 114, 423–429.

Pitzer, K.S., 1991. Ion inter action approach: theory and data correlation. In: Pitzer, K.S. (Ed.), Activity Coefficients in Electrolyte Solutions. CRC Press, Boca Raton, pp. 75–153.

Puşcaş, C.M., Onac, B.P., Tudor, T., 2010. The mineral assemblage of caves within Şălitrari Mountain (Cerna Valley, SW Romania): depositional environment and speleogenetic implications. Carbonates Evaporites 25, 107–115.

Qin, Y., Li, Y., Bao, H., Liu, F., Hou, K., Wan, D., Zhang, C., 2012. Massive atmospheric nitrate accumulations in a continental interior desert, northwestern China. Geology 40, 623–626.

RILEM PEM–25, 1980. Recommended tests to measure the deterioration of stone

and to assess the effectiveness of treatment methods. Mater. Struct. 13, 175–253.
Rijniers, L.A., Huinink, H.P., Pel, L., Kopinga, K., 2005. Experimental evidence of crystallization pressure inside porous media. Phys. Rev. Lett. 94, 075503(4).
Rodriguez-Navarro, C., Doehne, E., 1999. Salt weathering: influence of evaporation rate, supersaturation and crystallization pattern. Earth Surf. Process. Landf. 24, 191–209.
Rodriguez-Navarro, C., Doehne, E., Sebastian, E., 2000. How does sodium sulfate crystallize? Implications for the decay and testing of building materials. Cem. Concr. Res. 30, 1527–1534.
Saidov, T.A., Espinosa-Marzal, R.M., Pel, L., Scherer, G.W., 2012. Nucleation of sodium sulfate heptahydrate on mineral substrates studied by nuclear magnetic resonance. J. Cryst. Growth 338, 166–169.
Saidov, T.A., Pel, L., van der Heijden, G.H.A., 2015a. Crystallization of sodium sulfate in porous media by drying at a constant temperature. Int. J. Heat Mass Transf. 83, *621–628*.
Saidov, T.A., Pel, L., Kopinga, K., 2015b. Crystallization pressure of sodium sulfate heptahydrate. Cryst. Growth Des. 15, 2087–2093.
Schäfer, M., Steiger, M., 2002. A rapid method for the determination of cation exchange capacities of sandstones: preliminary data. Geol. Soc. Specif. Publ. 205, 431–439.
Scherer, G.W., 2004. Stress from crystallization of salt. Cem. Concr. Res. 34, 1613–1624.
Schiro, M., Ruiz-Agudo, E., Rodriguez-Navarro, C., 2012. Damage mechanism of porous materials due to in-pore salt crystallization. Phys. Rev. Lett. 109, 265503(5).
Schröder, W., 1929. Über das reziproke Salzpaar $MgSO_4$–$Na_2(NO_3)_2$–$H_2O$. II. Z. Anorg. Chem. 177, 71–85.
Schröder, W., 1930. Über das reziproke Salzpaar $MgSO_4$–$Na_2(NO_3)_2$–$H_2O$. V. Z. Anorg. Chem. 185, 153–166.
Shahidzadeh-Bonn, N., Rafaï, S., Bonn, D., Wegdam, G., 2008. Salt crystallization during evaporation: impact of interfacial properties. Langmuir 24, 8599–8605.
Snethlage, R., Wendler, E., 1997. Moisture cycles and sandstone degradation. In: Baer, N.S., Snethlage, R. (Eds.), Saving Our Architectural Heritage: Conservation of Historic Stone Structures. Wiley, Chichester, pp. 7–24.
Steiger, M., 2005. Crystal growth in porous materials–I: the crystallization pressure of large crystals. J. Cryst. Growth 282, 455–469.
Steiger, M., Asmussen, S., 2008. Crystallization of sodium sulfate phases in porous materials: the phase diagram $Na_2SO_4$–$H_2O$ and the generation of stress. Geochim. Cosmochim. Acta 72, 4291–4306.
Steiger, M., Linnow, K., Juling, H., Gülker, G., El Jarad, A., Brüggerhoff, S., Kirchner, D., 2008a. Hydration of $MgSO_4 \cdot H_2O$ and generation of stress in porous materials. Cryst. Growth Des. 8, 336–343.
Steiger, M., Kiekbusch, J., Nicolai, A., 2008b. An improved model incorporating Pitzer's equations for calculation of thermodynamic properties of pore solutions implemented into an efficient program code. Constr. Build. Mater. 22, 1841–1850.
Steiger, M., Charola, A.E., Sterflinger, K., 2015. Weathering and deterioration. In: Snethlage, R., Siegesmund, S. (Eds.), Stone in Architecture. Springer, Berlin, pp. 225–316.
Tsui, N., Flatt, R.J., Scherer, G.W., 2003. Crystallization damage by sodium sulfate. J. Cult. Herit. 4, 109–115.
Wexler, A.S., Seinfeld, J.H., 1991. Second generation inorganic aerosol model. Atmos. Environ. A 25, 2731–2748.